A prime advantage of monkeys is that they have a visual system that is almost identical to that in humans. They have eyes in the front of their head (not on the side like birds and rodents), a high resolution fovea in the center of the eye (rodents do not), and they move the eyes just as do humans.

Bob Wurtz

Which species do we use, and why?

"I'm searching for my keys."

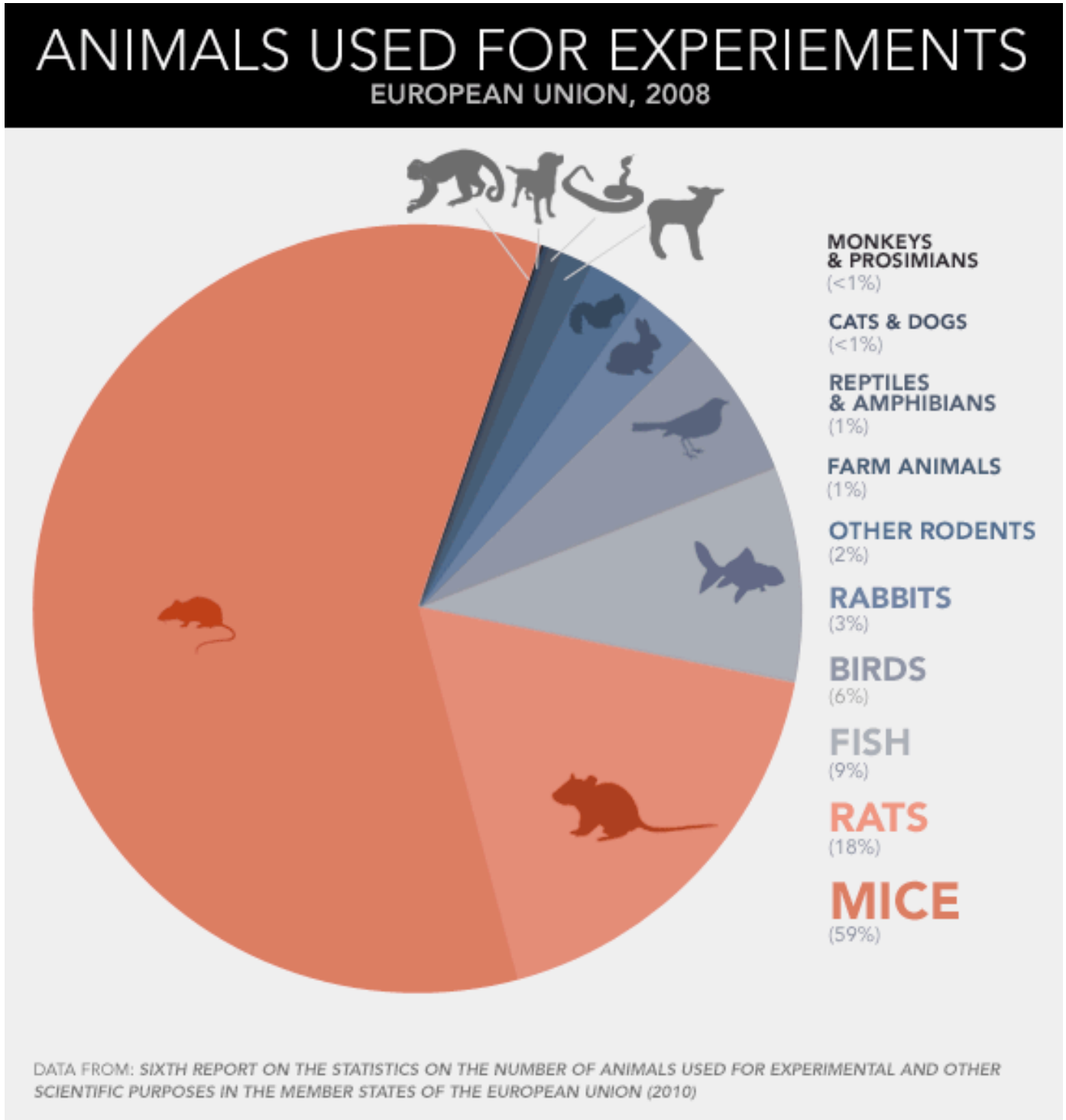
ANIMALS USED FOR EXPERIEMENTS
EUROPEAN UNION, 2008
MONKEYS & PROSIMIANS (<1%)
CATS & DOGS (<1%)
REPTILES & AMPHIBIANS (1%)
FARM ANIMALS (1%)
OTHER RODENTS (2%)
RABBITS (3%)
BIRDS (6%)
FISH (9%)
RATS (18%)
MICE (59%)
DATA FROM: SIXTH REPORT ON THE STATISTICS ON THE NUMBER OF ANIMALS USED FOR EXPERIMENTAL AND OTHER SCIENTIFIC PURPOSES IN THE MEMBER STATES OF THE EUROPEAN UNION (2010)

Engber, 2011

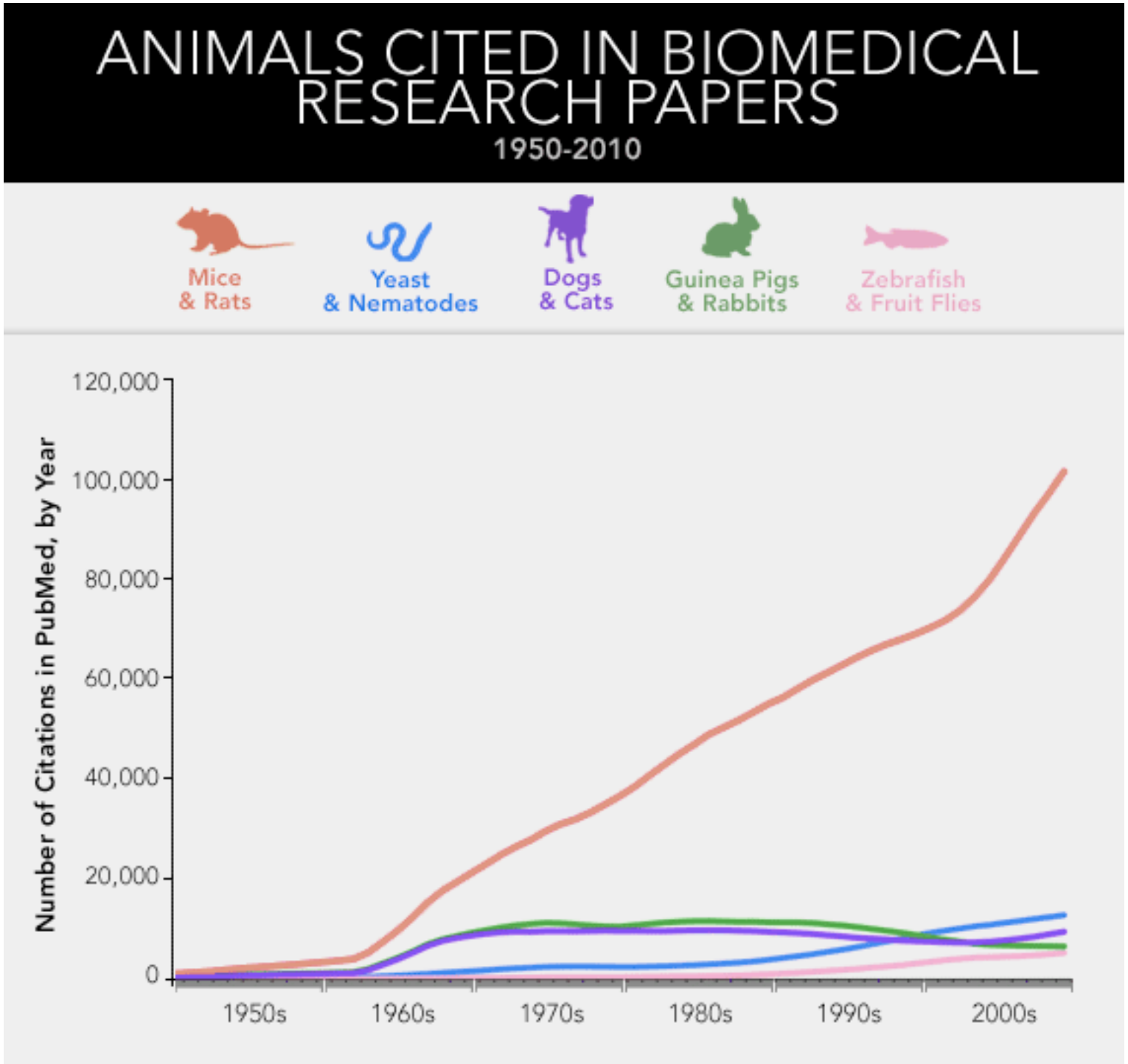
ANIMALS CITED IN BIOMEDICAL RESEARCH PAPERS
1950-2010
Mice & Rats
Yeast & Nematodes
Dogs & Cats
Guinea Pigs & Rabbits
Zebrafish & Fruit Flies
Number of Citations in PubMed, by Year
120,000
100,000
80,000
60,000
40,000
20,000
0
1950s
1960s
1970s
1980s
1990s
2000s

Engber, 2011

Sensory representations through mammalian evolution

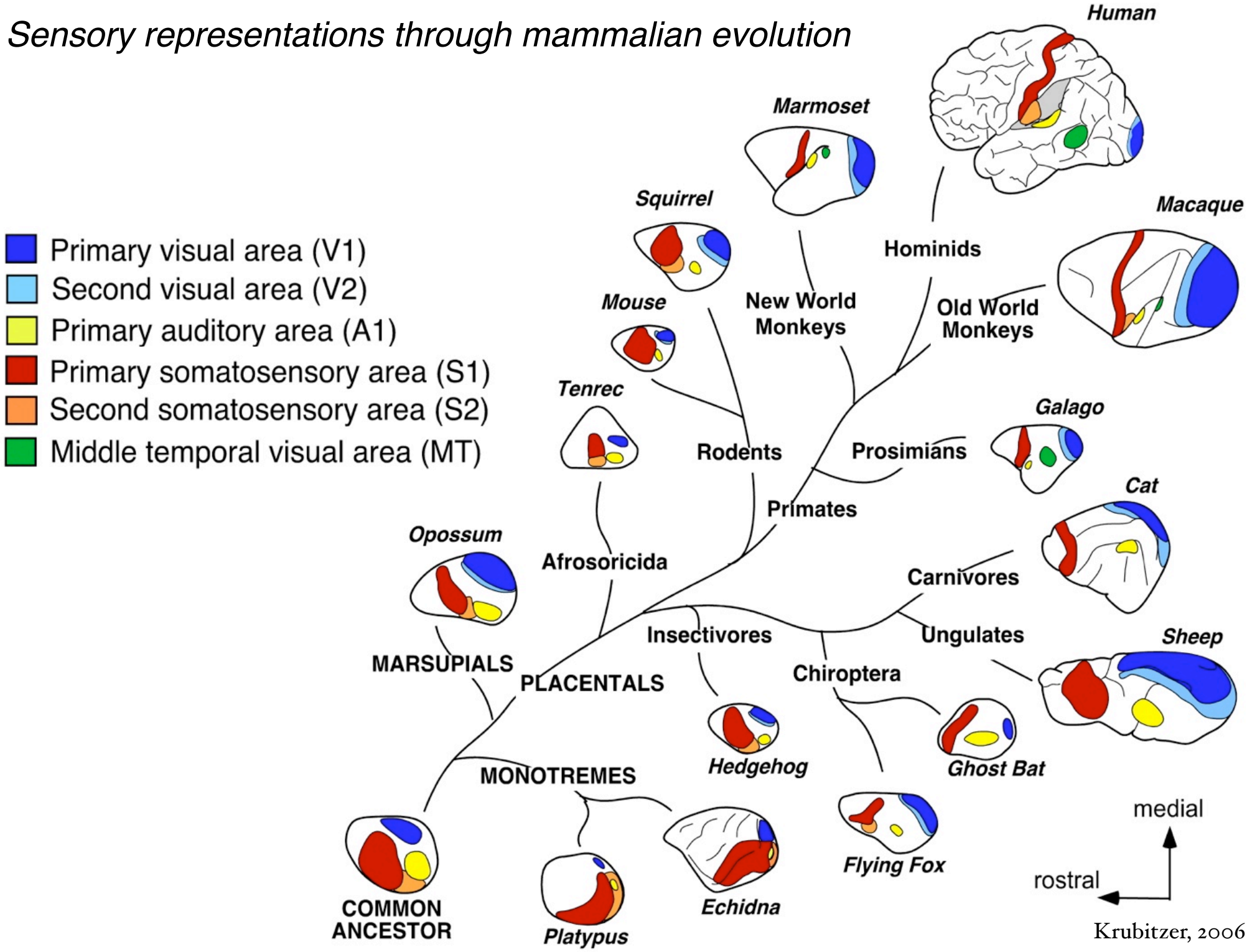

Krubitzer, 2006

Retina

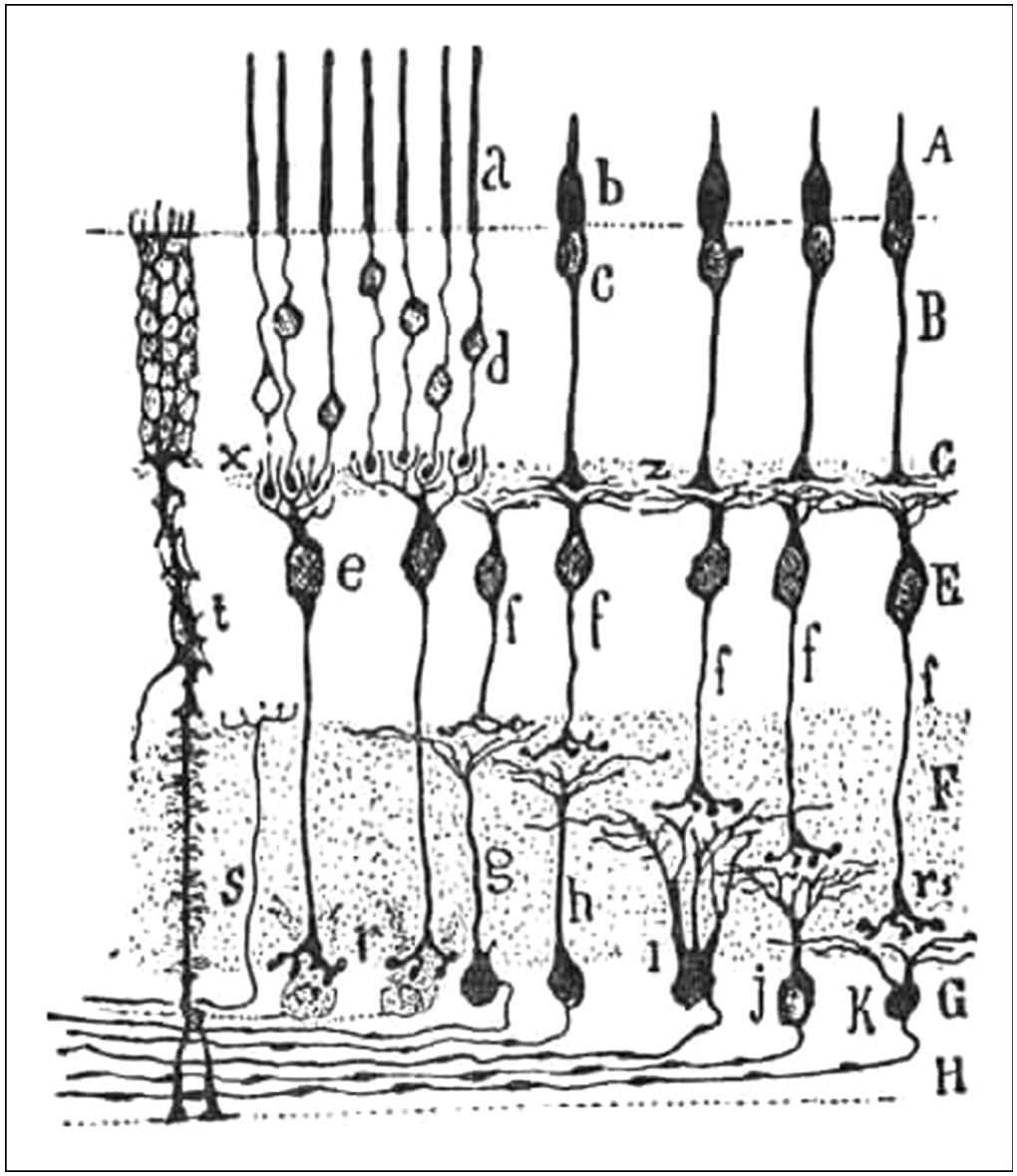

FIG. 45. Scheme of the structure of the retina. *A*, layer of rods and cones; *a*, rods; *b*, cones; *E*, layer of bipolar cells; *G*, layer of large ganglion cells; *H*, layer of nerve fibres; *s*, centrifugal nerve fibre. (Barker after Ramón y Cajal.)

Retinal cell type diversity and circuit specificity

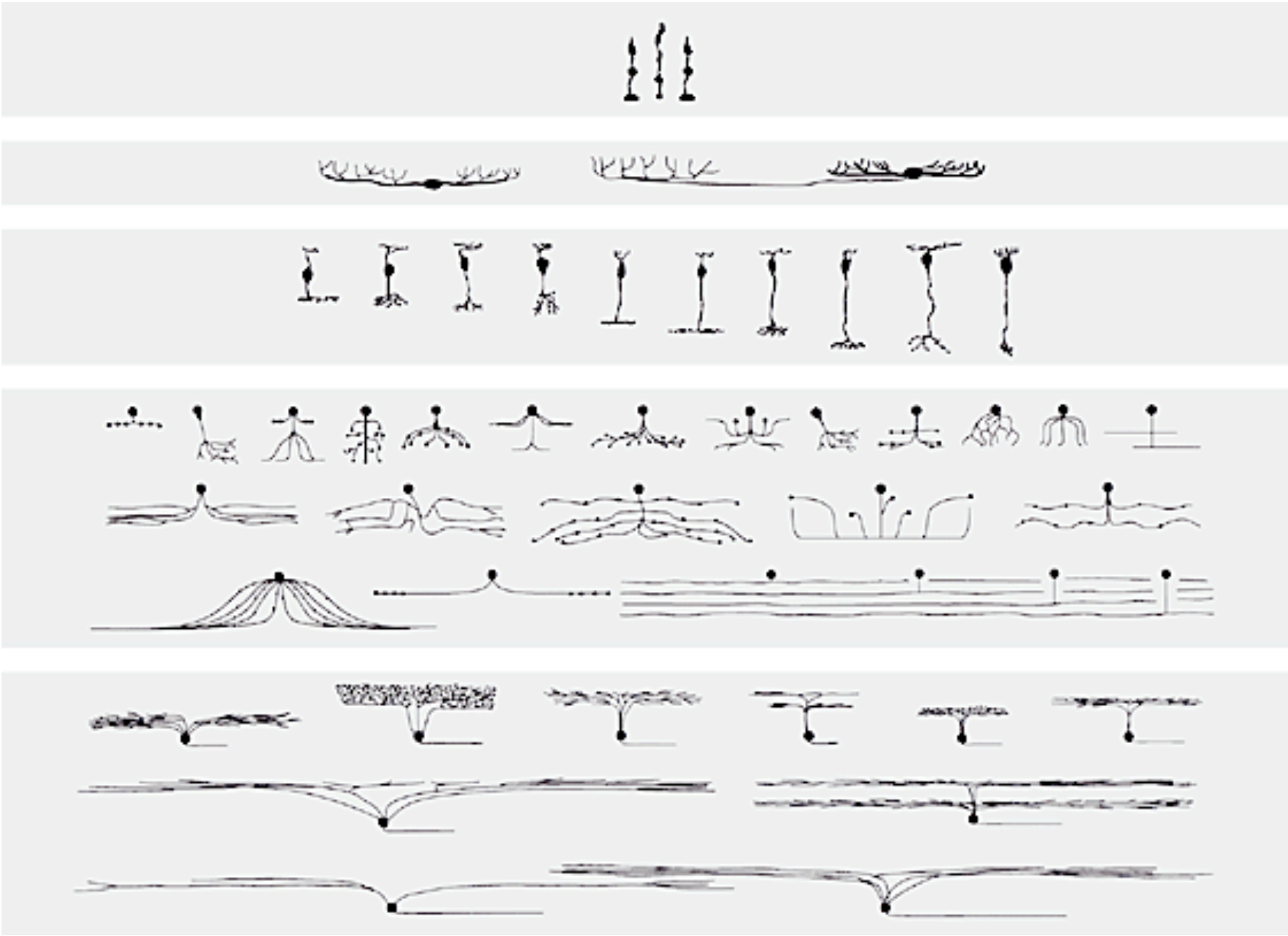

Masland, 2001

Diversity of ganglion cell morphology in retina

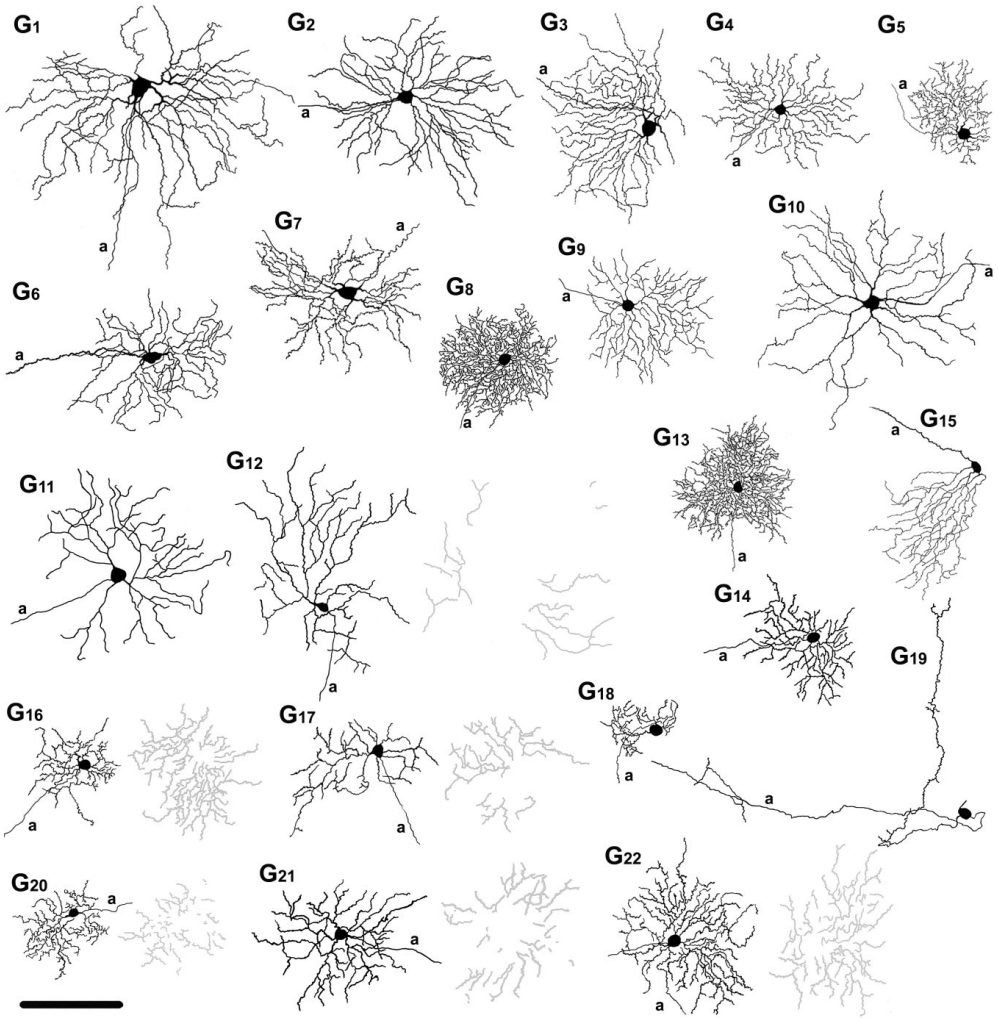

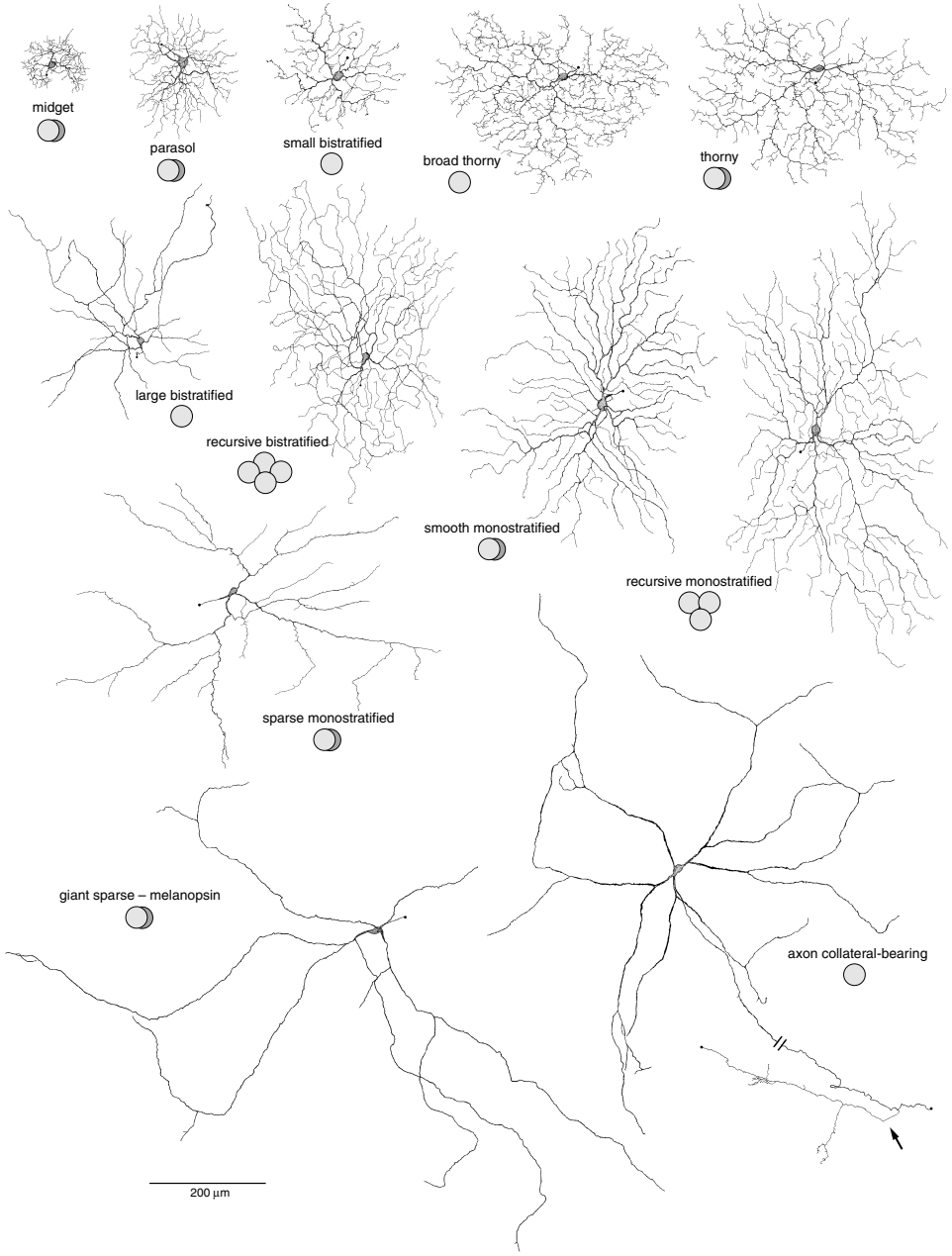

The distribution of rods and cones in human retina

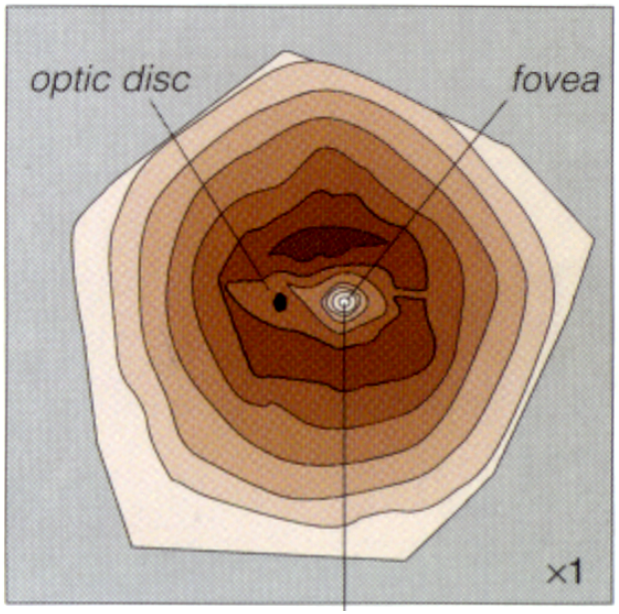

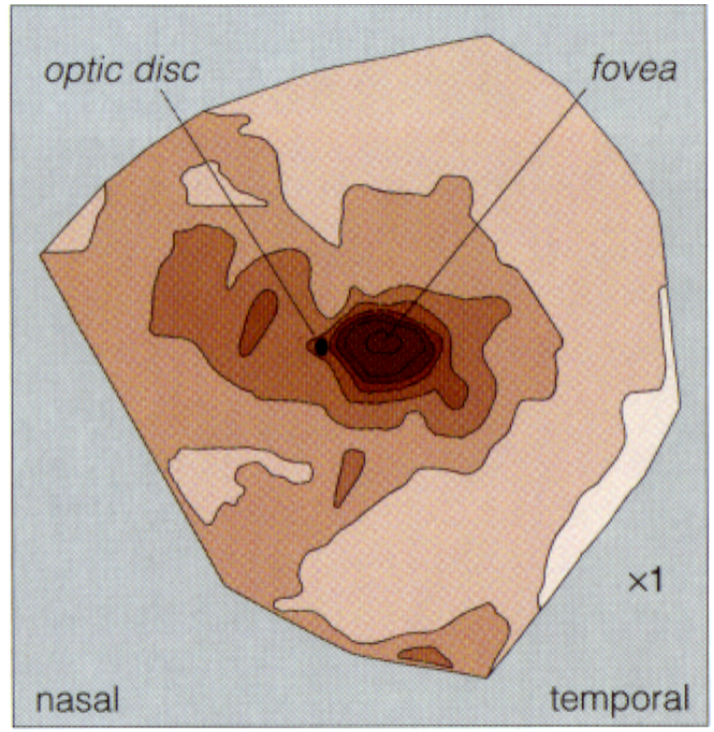

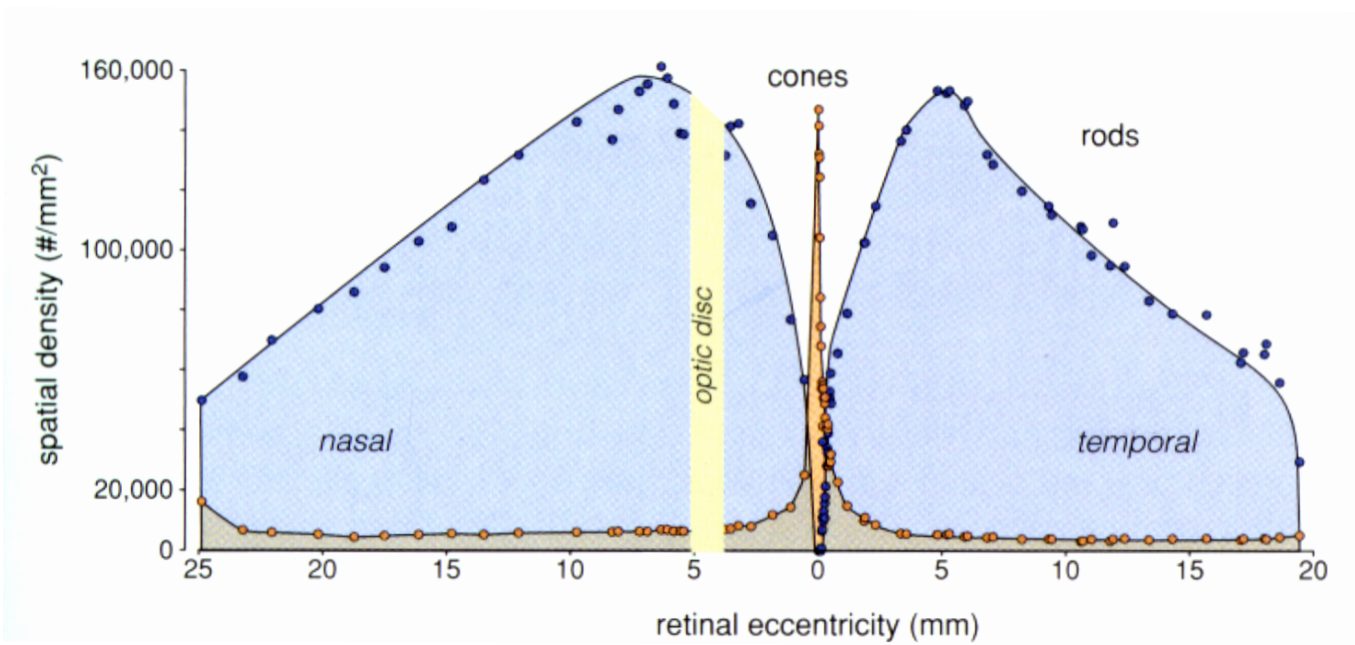

Sampling of visual space by human retinal ganglion cells

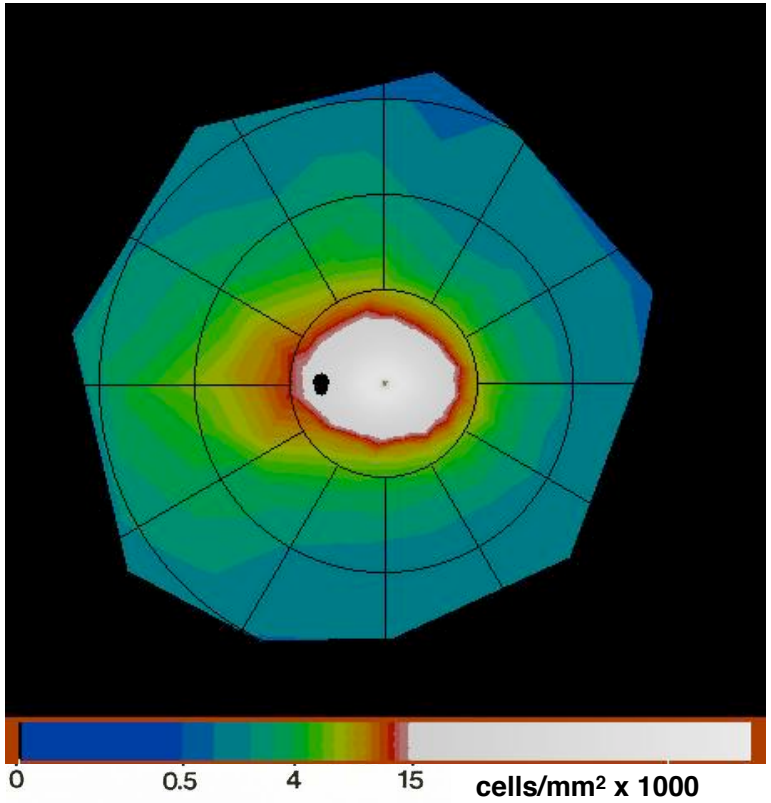

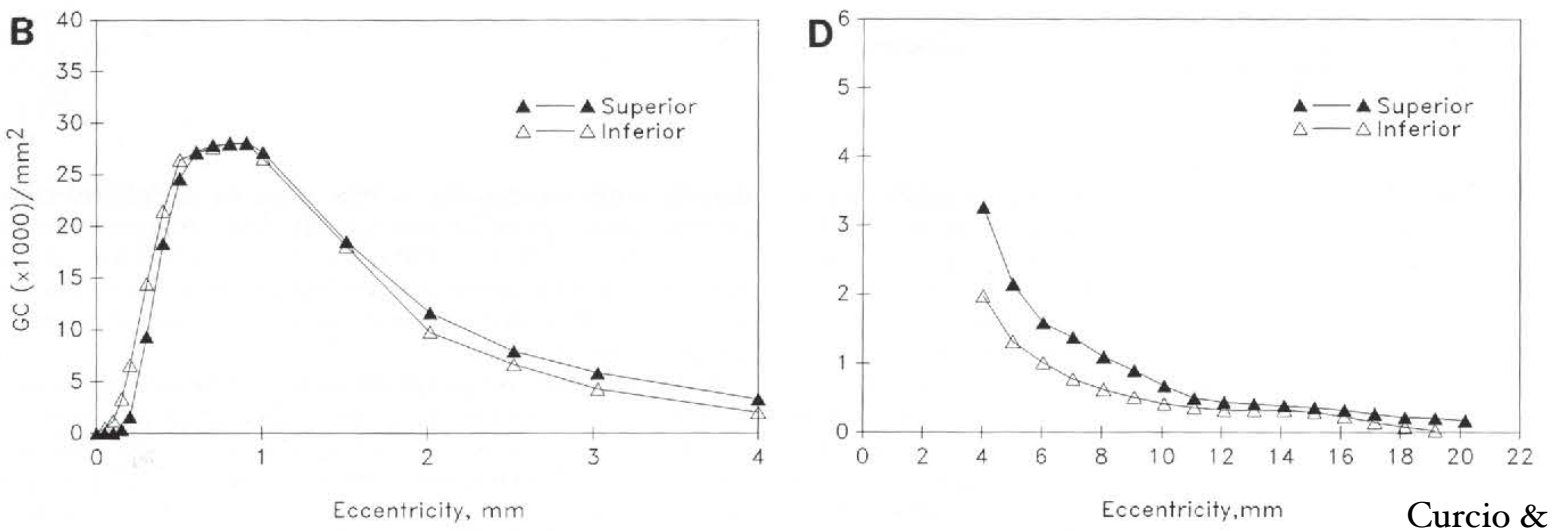

Curcio & Allen, 1990

Sampling of visual space by different mouse ganglion cell types

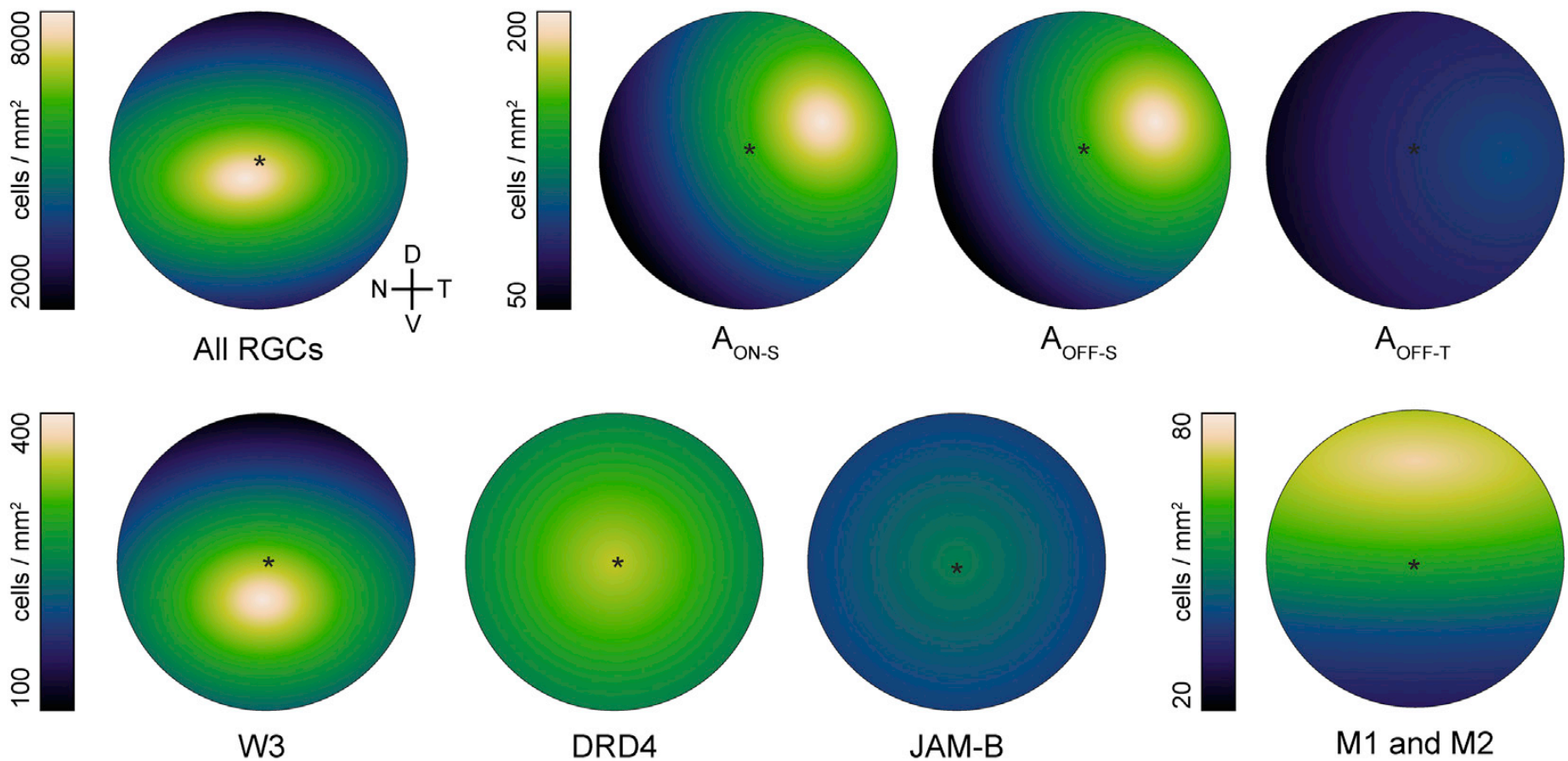

Bleckert et al, 2014

Diversity of ganglion cell morphology in mammalian retina

Icon	Mouse	Rabbit	Cat	Macaque	Properties

A catalog of retinal ganglion cell types in the mammalian retina[a]

Icon	Mouse	Rabbit	Cat	Macaque	Properties
	M1[1,2]			Outer melanopsin[3]	Large sparse dendrites. ON sluggish synaptic response.
	M2[1,2]			Inner melanopsin[3]	Large complex dendrites. ON sluggish synaptic response.
	ON DS temporal[4]	ON DS temporal[5]			ON DS. Preferred direction temporal.
	ON DS ventral,[4] Spig-1 EGFP[6,7]	ON DS ventral[5]			ON DS. Preferred direction ventral.
	ON, DS dorsal[4,6,7]	ON DS dorsal[5]			ON DS. Preferred direction dorsal.
	ON–OFF DS temporal[9]	ON–OFF DS temporal[9]	Theta?[10]	Recursive bistratified?[11]	ON-OFF DS. Preferred direction temporal.
	ON-OFF DS dorsal[9]	ON-OFF DS dorsal[9]	Theta?[10]	Recursive bistratified?[11]	ON-OFF DS. Preferred direction dorsal.
	Drd4-EGFP,[12] W9[8]	ON–OFF, DS nasal[9]	Theta?[10]	Recursive bistratified?[11]	ON-OFF DS. Preferred direction nasal.
	BD-CreER,[8] Hb9-EGFP[13]	ON–OFF, DS ventral[9]	Theta?[10]	Recursive bistratified?[11]	ON-OFF DS. Preferred direction ventral. Asymmetric dendrites in mouse.
	JAM-B[14]	OFF coupled[15], G3[16]			OFF DS. Preferred direction ventral. Highly asymmetric dendrites point ventral.

A catalog of retinal ganglion cell types in the mammalian retina[a] *(Continued)*

Icon	Mouse	Rabbit	Cat	Macaque	Properties
	ON alpha,[17] PV-Cre-1[18]	ON alpha[19]	ON alpha[20,21]		Large dendritic field. ON response.
	PV-Cre-3[18]	ON parasol[15]		ON parasol[22]	Medium dendritic field. ON response.
				ON smooth[23]	
		ON beta[15]	ON beta[24]		Small dendritic field. ON response.
				ON midget[22]	Small dendritic field. ON response.
		OFF beta[15]	OFF beta[24]		Small dendritic field. OFF response.
				OFF midget[22]	Small dendritic field. OFF response.
	PV-Cre-4[18]	OFF parasol[15]	Eta?[25]	OFF parasol[22]	Medium dendritic field. OFF response.
	OFF alpha transient[17], PV-Cre-5[18]	OFF alpha[19]	OFF alpha[24]	OFF smooth[23]	Large dendritic field. OFF response.
	OFF alpha Sustained,[17] PV-Cre-6[18]	OFF delta[15]	OFF delta[19]		Large dendritic field. OFF sustained response.

A catalog of retinal ganglion cell types in the mammalian retina[a] *(Continued)*

Icon	Mouse	Rabbit	Cat	Macaque	Properties
		ON-bistratified?[15]		Small-bistratified[11]	ON excitation, OFF inhibition, blue-yellow opponent in macaque.
				Large-bistratified[11]	Blue-yellow opponent.
	W3[26]	Local edge Detector[5,27]	Zeta[28]	Broad thorny[11]	ON–OFF, strong surround, fast ON–OFF inhibition.
			Epsilon?[29]	Recursive monostratified[11]	
				ON narrow thorny[11]	
				OFF narrow thorny[11]	
		Uniformity Detector[30]	Uniformity Detector[31]		Transiently suppressed by visual stimuli. ON-OFF response. Dendrites just outside the ChAT bands.

[a]Each graphic icon illustrates stratification of the dendritic tree in the IPL, divided into 10 laminae (Siegert et al., 2009). For each type we list the defining morphological and physiological features and identify its plausible correspondences in four species, as supported by the cited literature. For further detail on cross-species comparisons, see Berson (2008). Note that many of these ganglion cell types have only sparse and partial entries, emphasizing the need for future work to round out the catalog of retinal output signals.

References: [1]Hattar et al. (2006). [2]Schmidt et al. (2011b). [3]Dacey et al. (2005). [4]Sun et al. (2006). [5]Barlow, Hill, & Levick (1964), but see Kanjhan & Sivyer (2010) and Hoshi et al. (2011) for finer divisions. [6]Yonehara et al. (2009). [7]Yonehara et al. (2008). [8]Kay et al. (2011). [9]Oyster & Barlow (1967). [10]Isayama, Berson, & Pu (2000). [11]Dacey (2004). [12]Huberman et al. (2009). [13]Trenholm et al. (2011) erroneously identified the preferred direction as temporal. [14]Kim et al. (2008). [15]Roska, Molnar, & Werblin (2006). [16]Hoshi et al. (2011). [17]Pang, Gao, & Wu (2003). [18]Münch et al. (2009). [19]Zhang et al. (2005). [20]Cleland, Levick, & Wässle (1975). [21]Wässle, Peichl, & Boycott (1981). [22]Dacey & Packer (2003). [23]Crook et al. (2008). [24]Wässle, Boycott, & Illing (1981). [25]Berson, Isayama, & Pu (1999). [26]Kim et al. (2010). [27]van Wyk, Taylor, & Vaney (2006). [28]Berson, Pu, & Famiglietti (1998). [29]Pu, Berson, & Pan (1994). [30]Sivyer & Vaney (2010). [31]Cleland & Levick (1974).

Roska and Meister, 2014

Diversity of ganglion cell morphology in mammalian retina

Icon	Mouse	Rabbit	Cat	Macaque	Properties
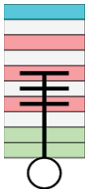				ON midget[22]	Small dendritic field. ON response.
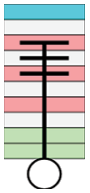				OFF midget[22]	Small dendritic field. OFF response.

Roska and Meister, 2014

Diversity of ganglion cell morphology and function in macaque retina

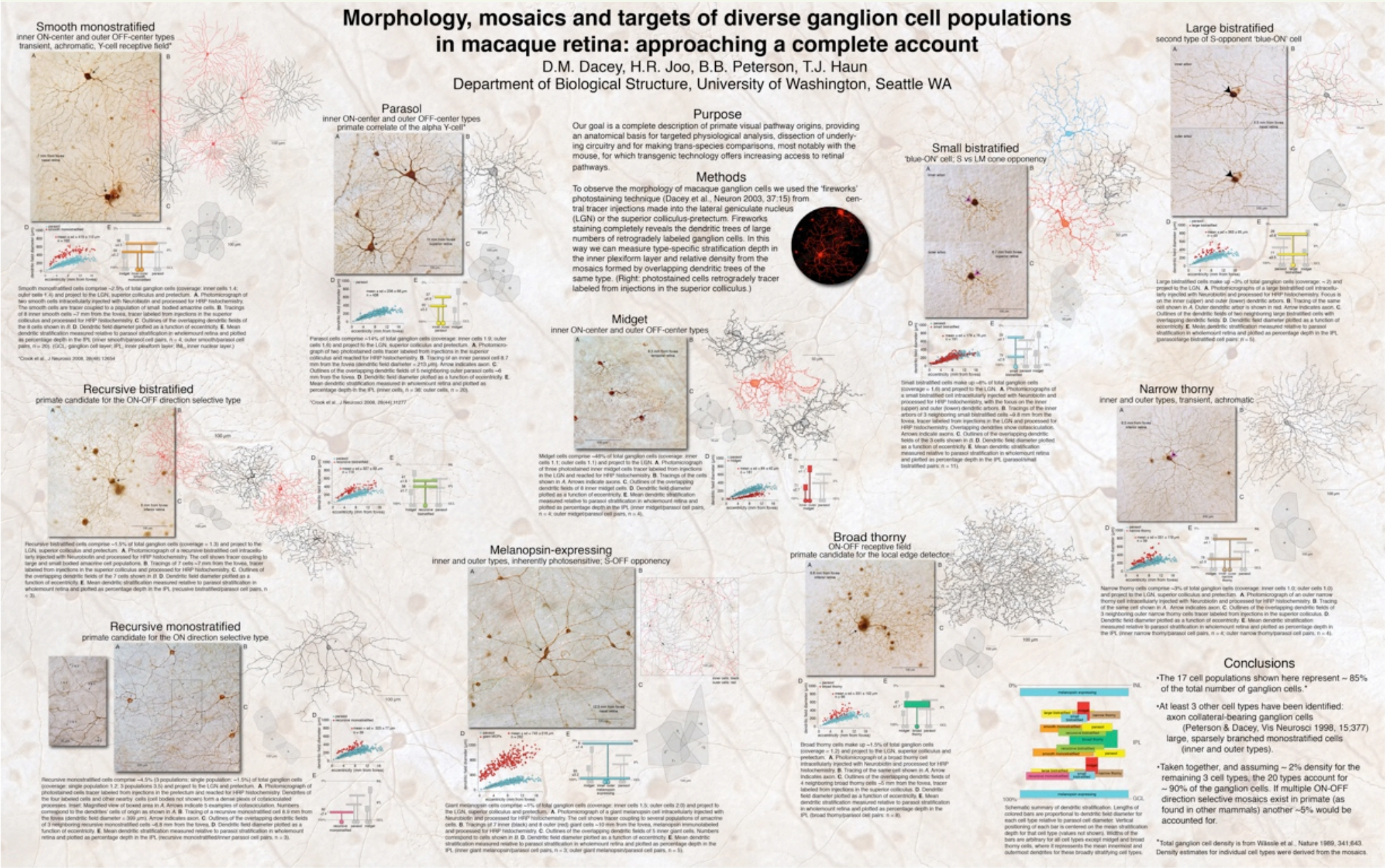

Dacey et al., 2010

Midget cells are about half of all primate ganglion cells

Midget

inner ON-center and outer OFF-center types

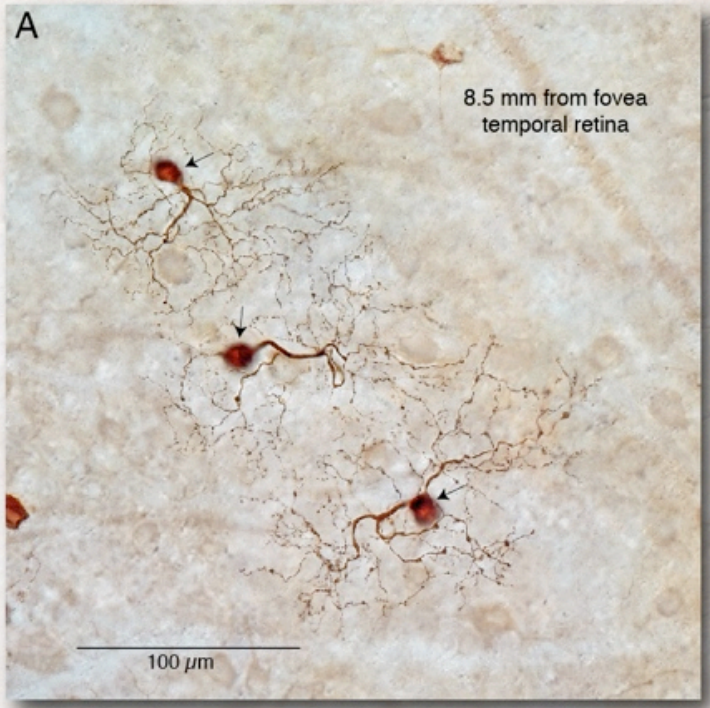

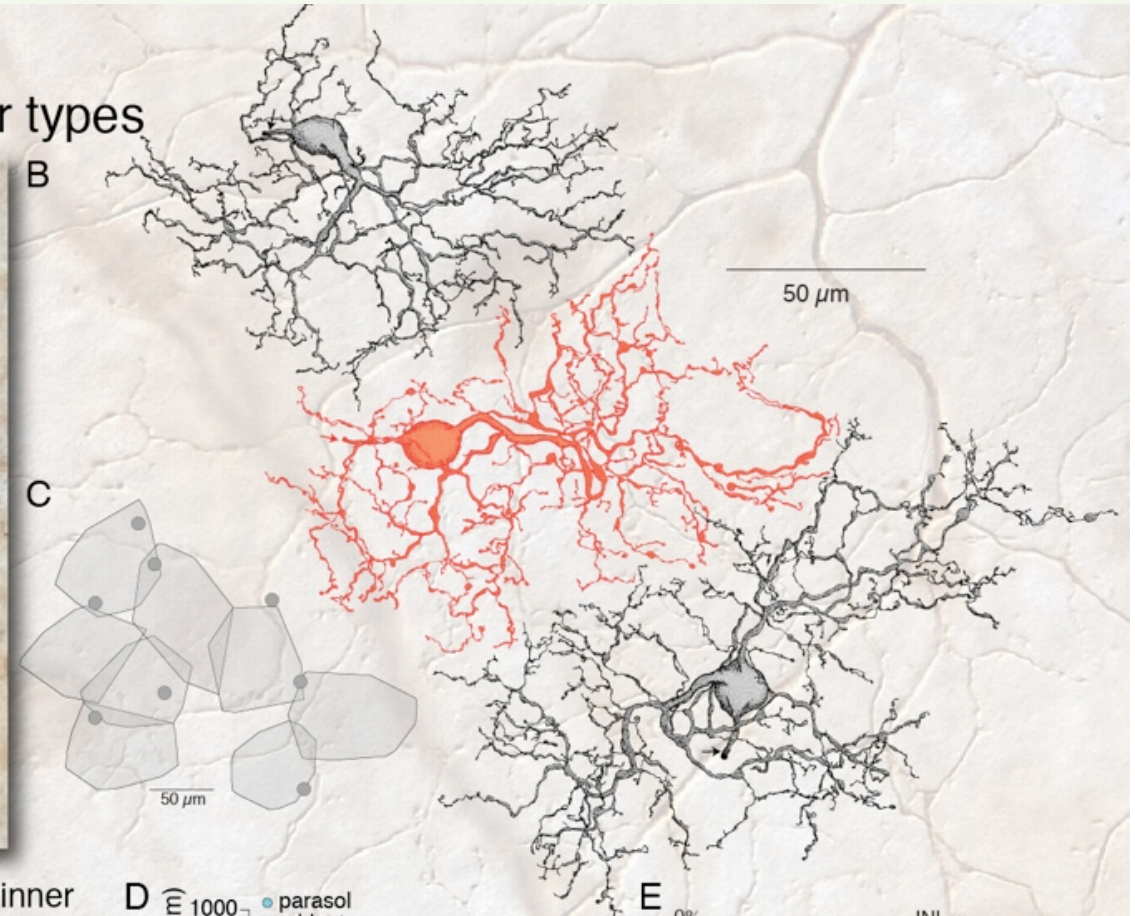

Midget cells comprise ~46% of total ganglion cells (coverage: inner cells 1.1; outer cells 1.1) and project to the LGN. **A**. Photomicrograph of three photostained inner midget cells tracer labeled from injections in the LGN and reacted for HRP histochemistry. **B**. Tracings of the cells shown in *A*. Arrows indicate axons. **C**. Outlines of the overlapping dendritic fields of 8 inner midget cells. **D**. Dendritic field diameter plotted as a function of eccentricity. **E**. Mean dendritic stratification measured relative to parasol stratification in wholemount retina and plotted as percentage depth in the IPL (inner midget/parasol cell pairs, n = 4; outer midget/parasol cell pairs, n = 4).

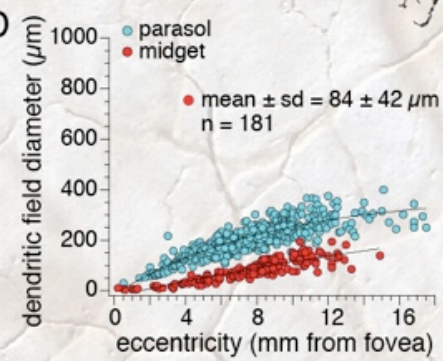

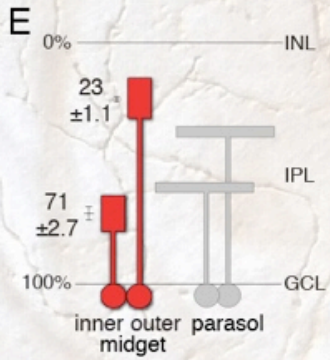

Dacey et al., 2010

Color-opponent midget cells: a primate specialization

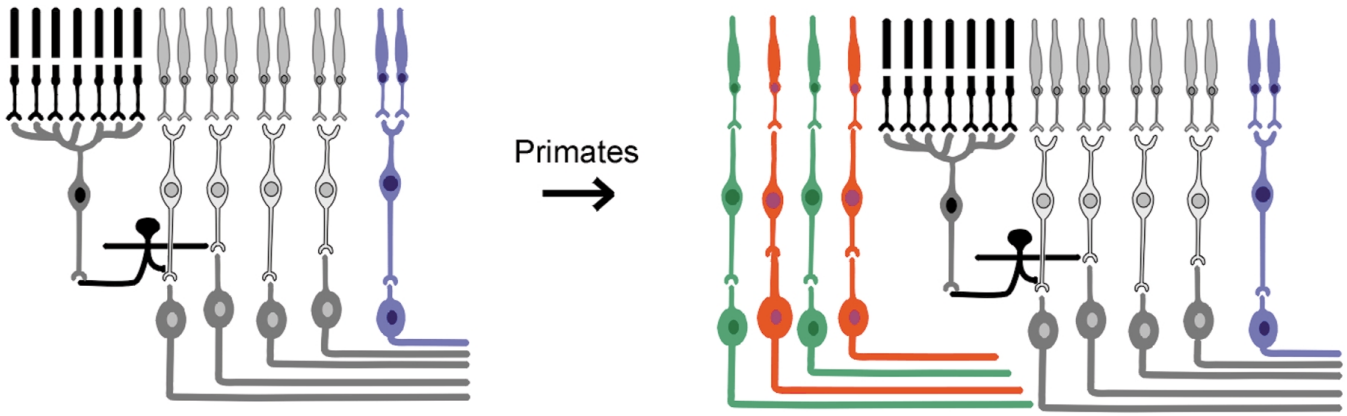

Generic mammalian retina

Primate Color Opponent Ganglion Cells

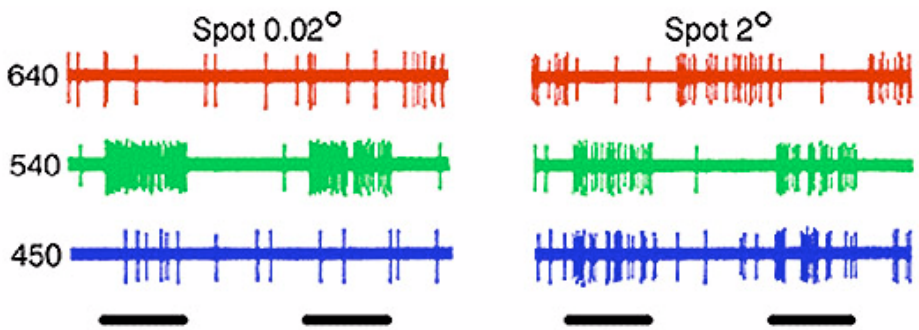

DeMonasterio & Gouras (1975)

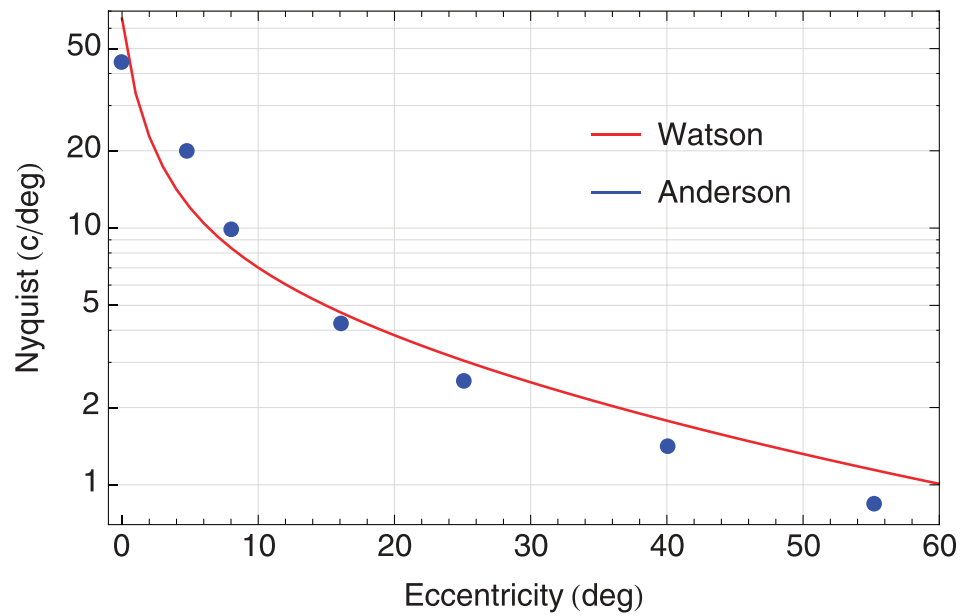

Inferred Receptive Field Description

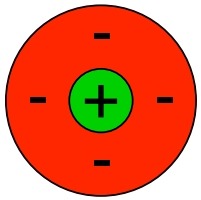

Masland, 2001;
DeMonasterios & Gouras, 1975;
Watson, 2014

Diversity of ganglion cell morphology in mammalian retina

Icon	Mouse	Rabbit	Cat	Macaque	Properties
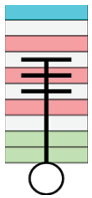	W3[26]	Local edge Detector[5,27]	Zeta[28]	Broad thorny[11]	ON–OFF, strong surround, fast ON–OFF inhibition.

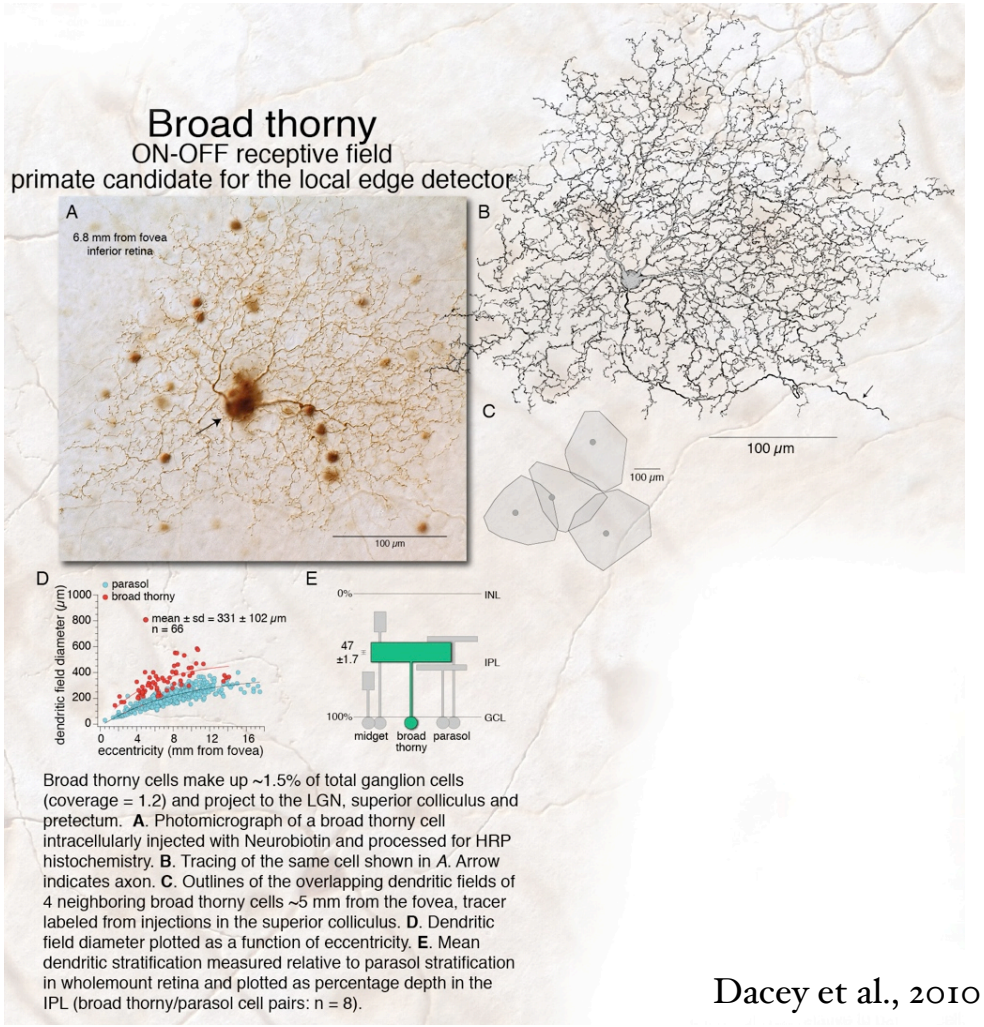

Dacey et al., 2010

Roska and Meister, 2014

The most numerous ganglion cell type of the mouse retina is a selective feature detector

Yifeng Zhang[1], In-Jung Kim[2], Joshua R. Sanes[3], and Markus Meister[3,4]

Department of Molecular and Cellular Biology, Center for Brain Science, Harvard University, Cambridge, MA 02138

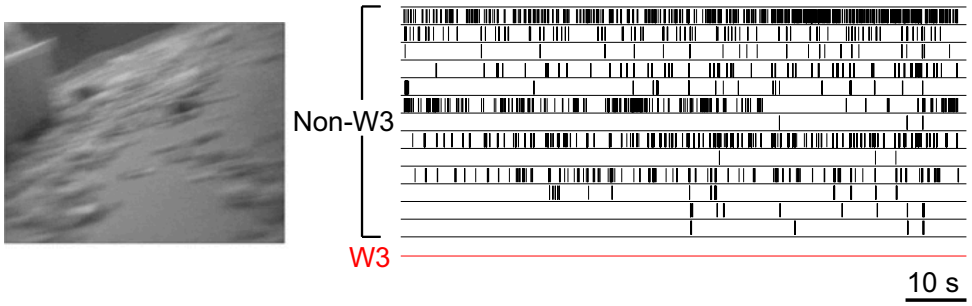

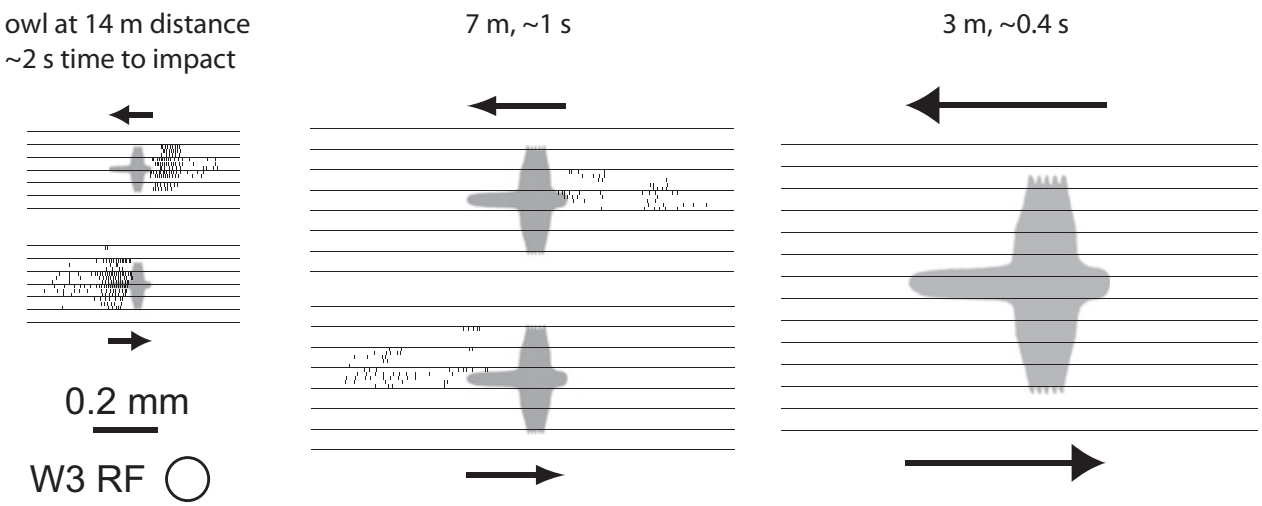

Zhang et al., 2012

Cones

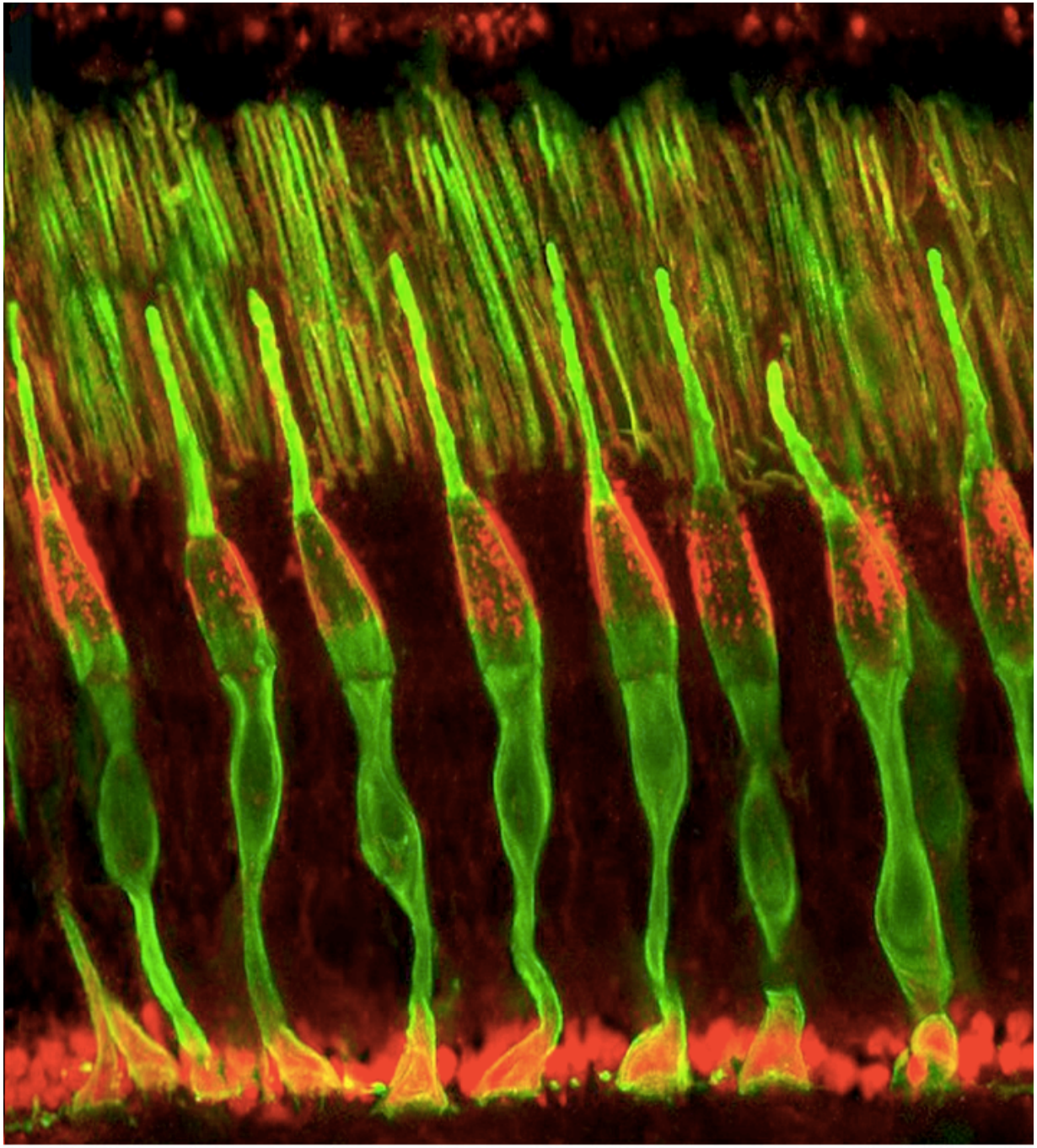

Cuenca, 2009

Most mouse cones express two opsins in a regionally varying pattern

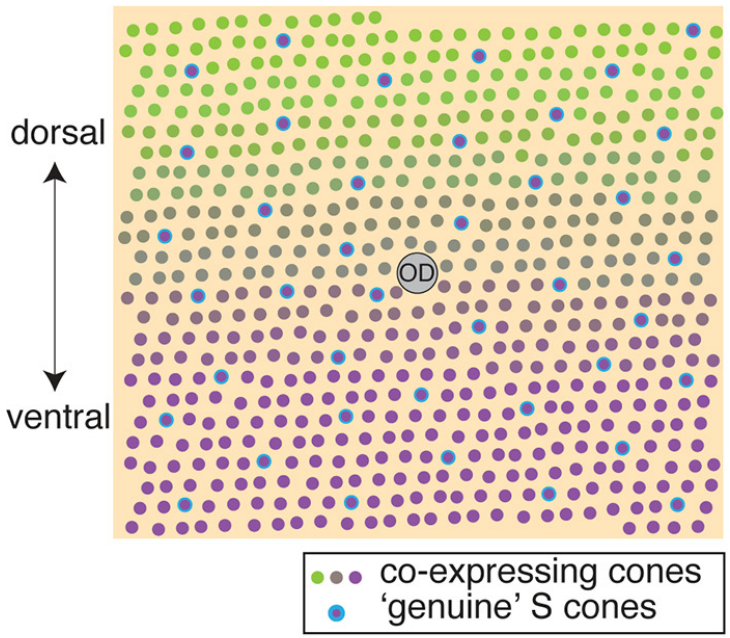

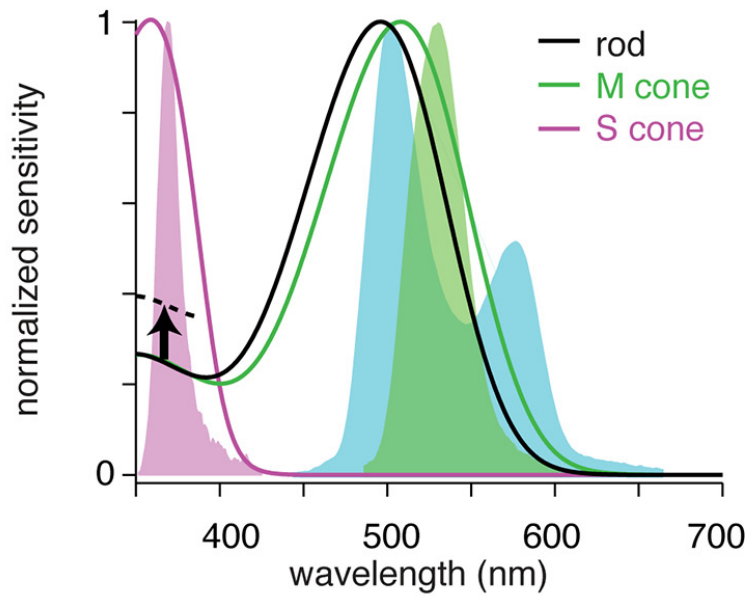

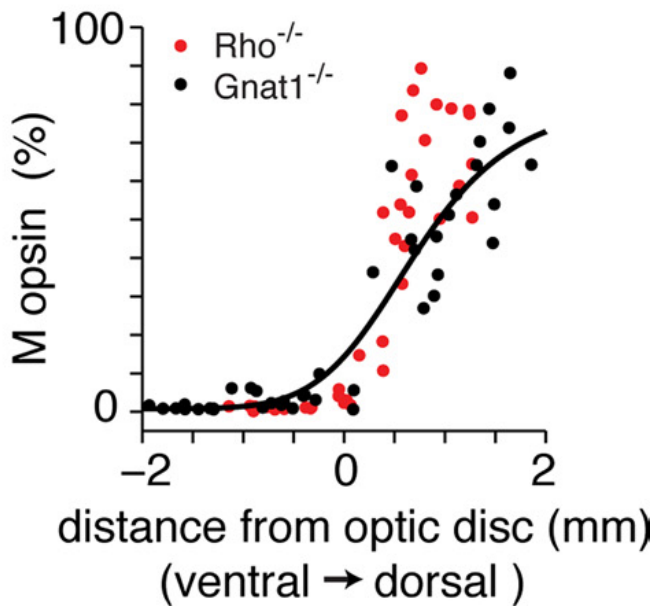

Wang, Weick & Demb, 2011

All retinas are not the same

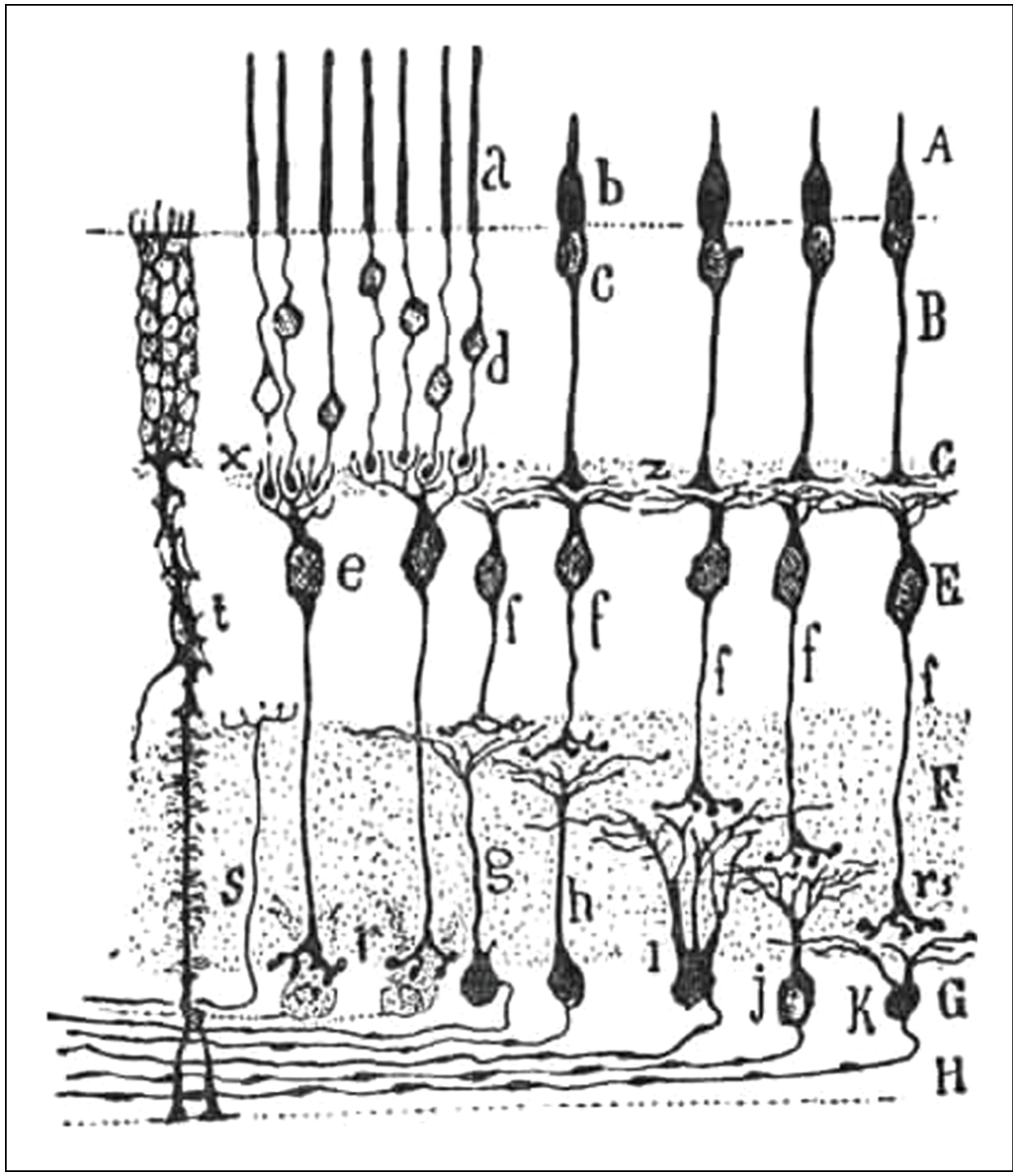

FIG. 45. Scheme of the structure of the retina. *A*, layer of rods and cones; *a*, rods; *b*, cones; *E*, layer of bipolar cells; *G*, layer of large ganglion cells; *H*, layer of nerve fibres; *s*, centrifugal nerve fibre. (Barker after Ramón y Cajal.)

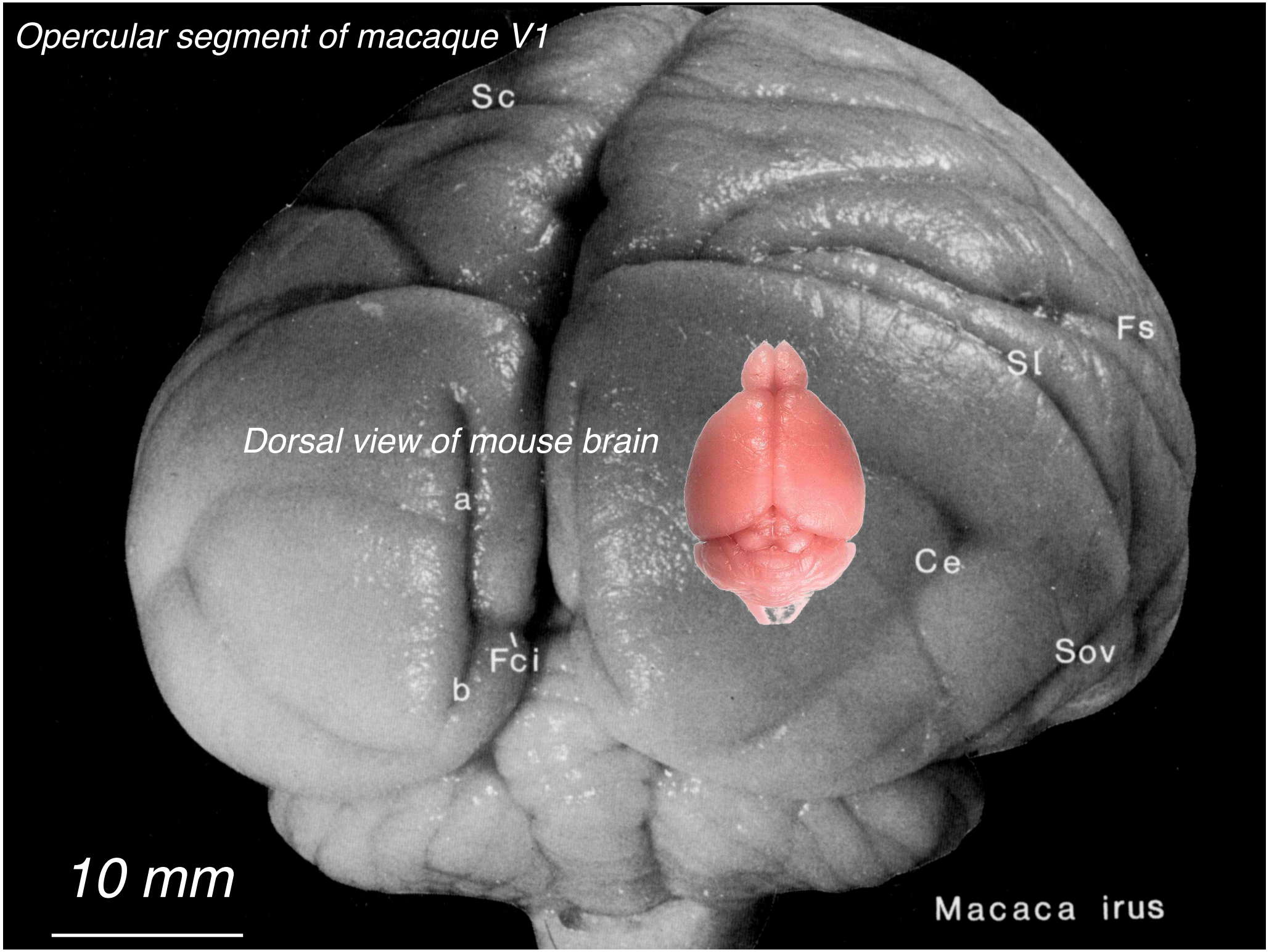
Opercular segment of macaque V1
Sc
Fs
Sl
Dorsal view of mouse brain
a
Ce
Fci
Sov
b
10 mm
Macaca irus

Visuotopic organization of macaque V1

The entire mouse brain is the same size as the representation of the central 2 deg of visual field in macaque V1

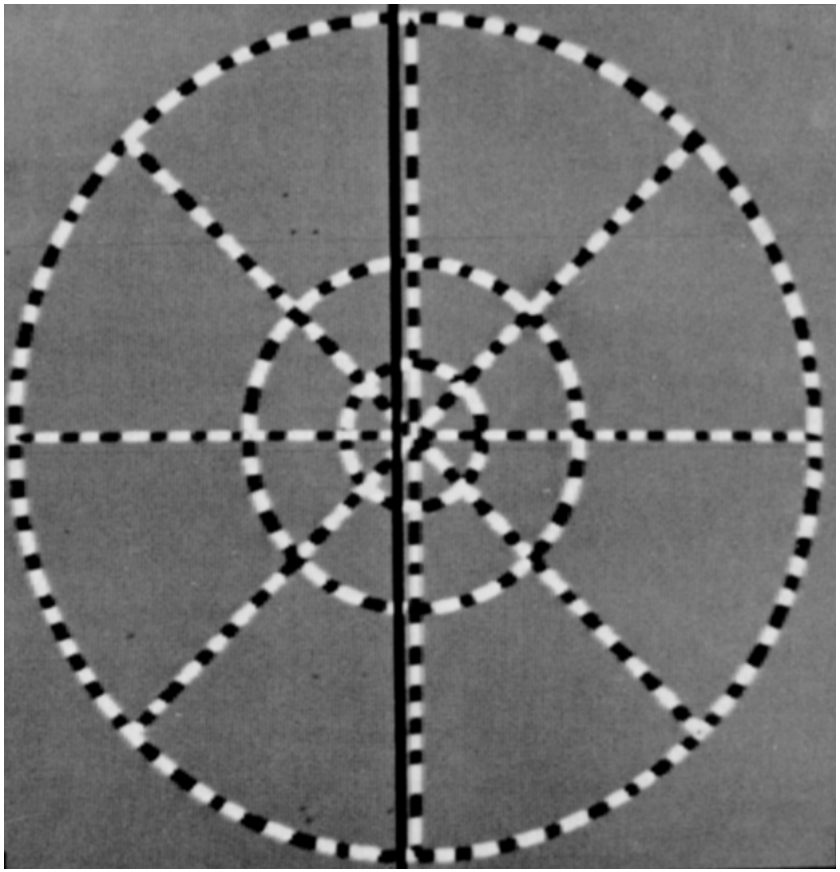

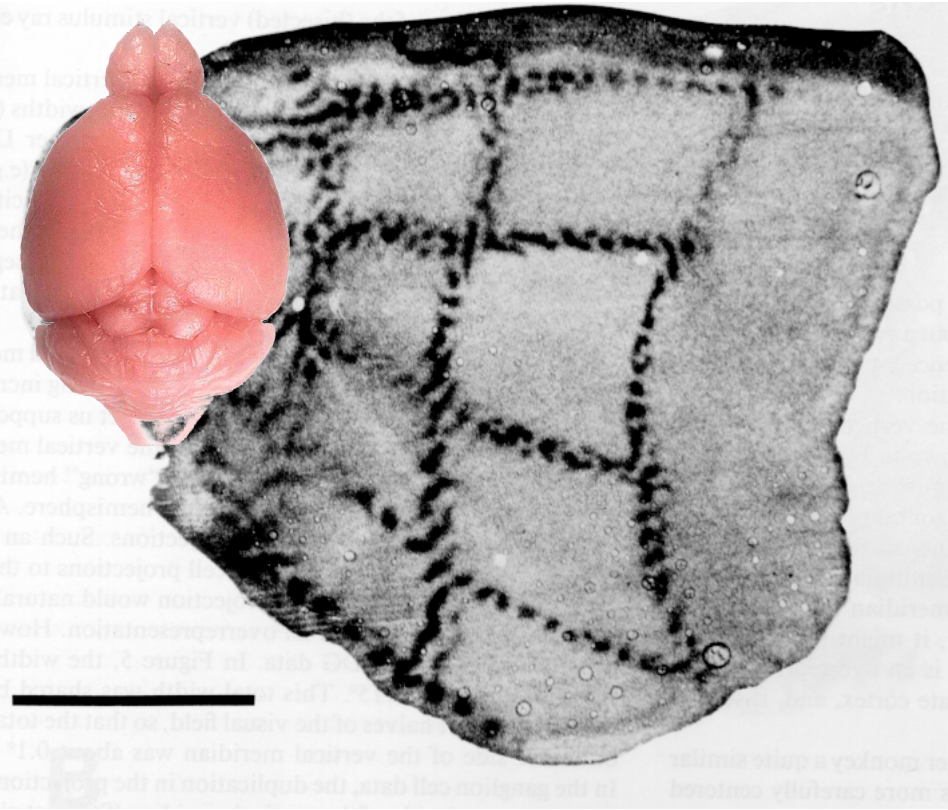

Tootell, Silverman, Switkes and DeValois, 1982

Monkey vision

Johannes Burge

Mouse vision

Johannes Burge

Magnification factor and binocularity

Mouse

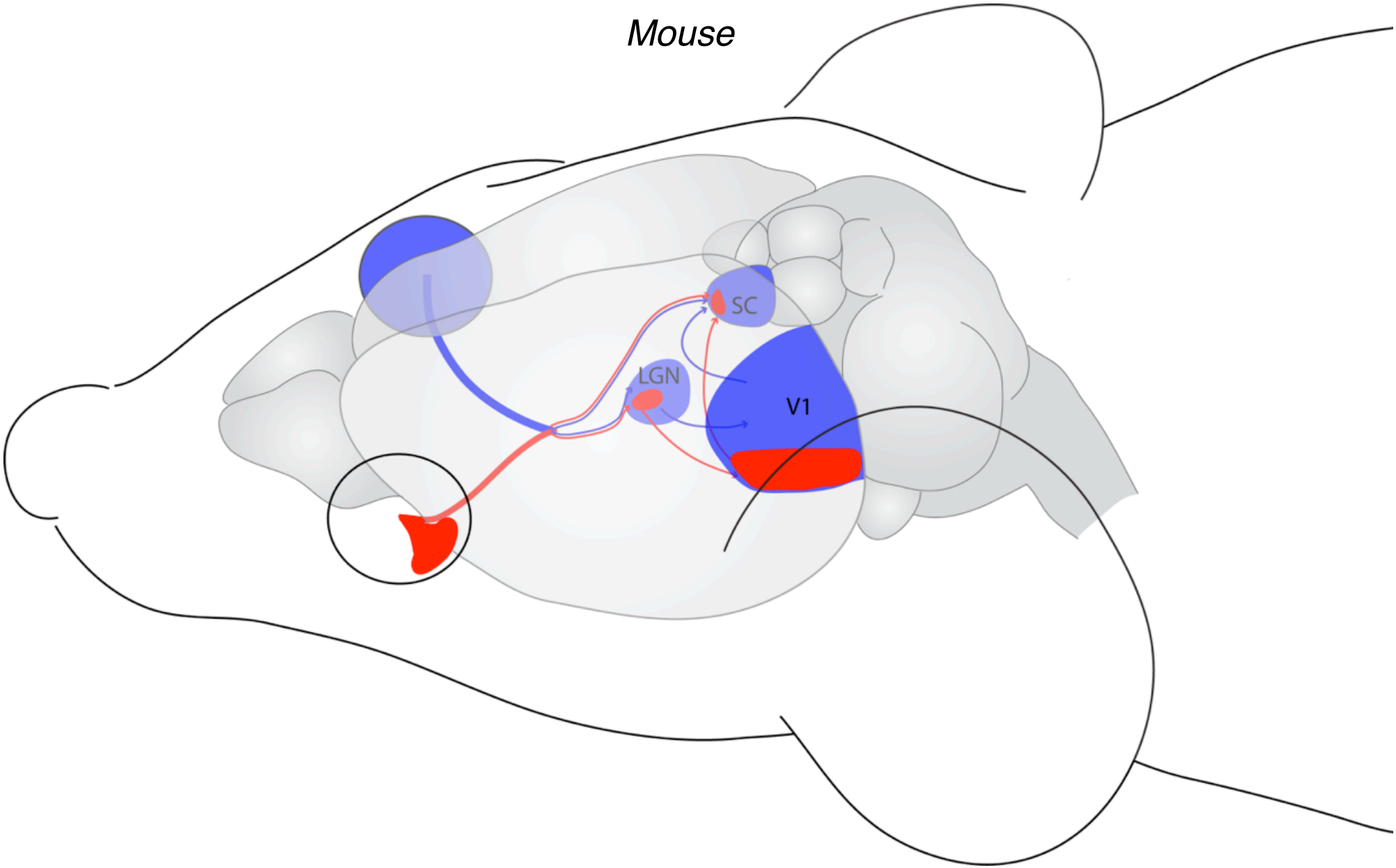

Wilks, Harvey & Rodger, 2013

Magnification factor and binocularity

Macaque

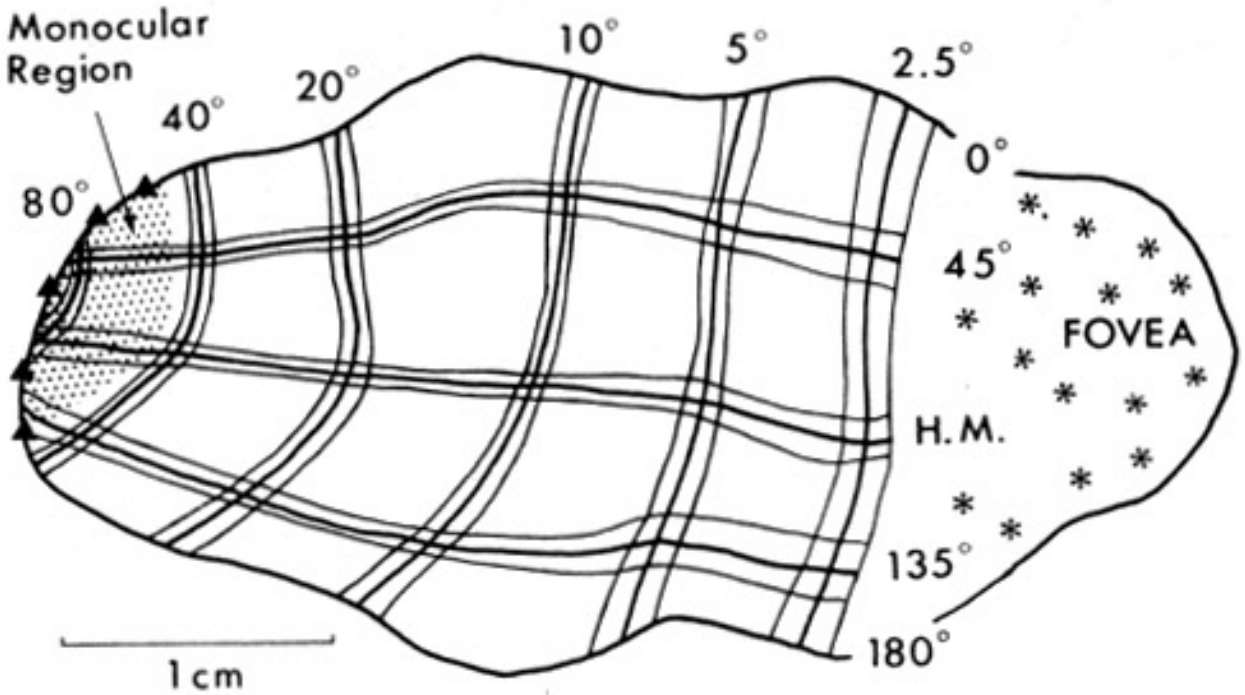

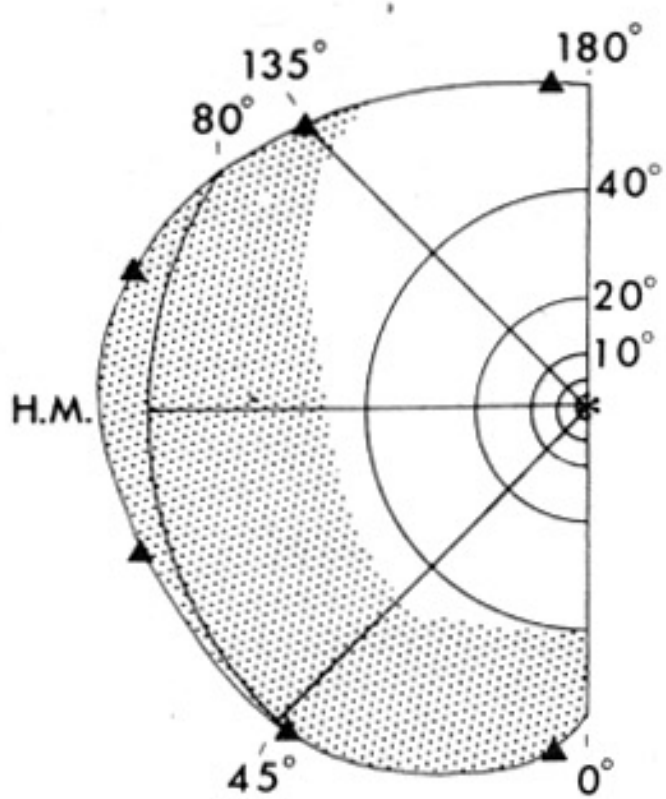

Van Essen, Newsome & Maunsell, 1981

Monocular deprivation – monkey

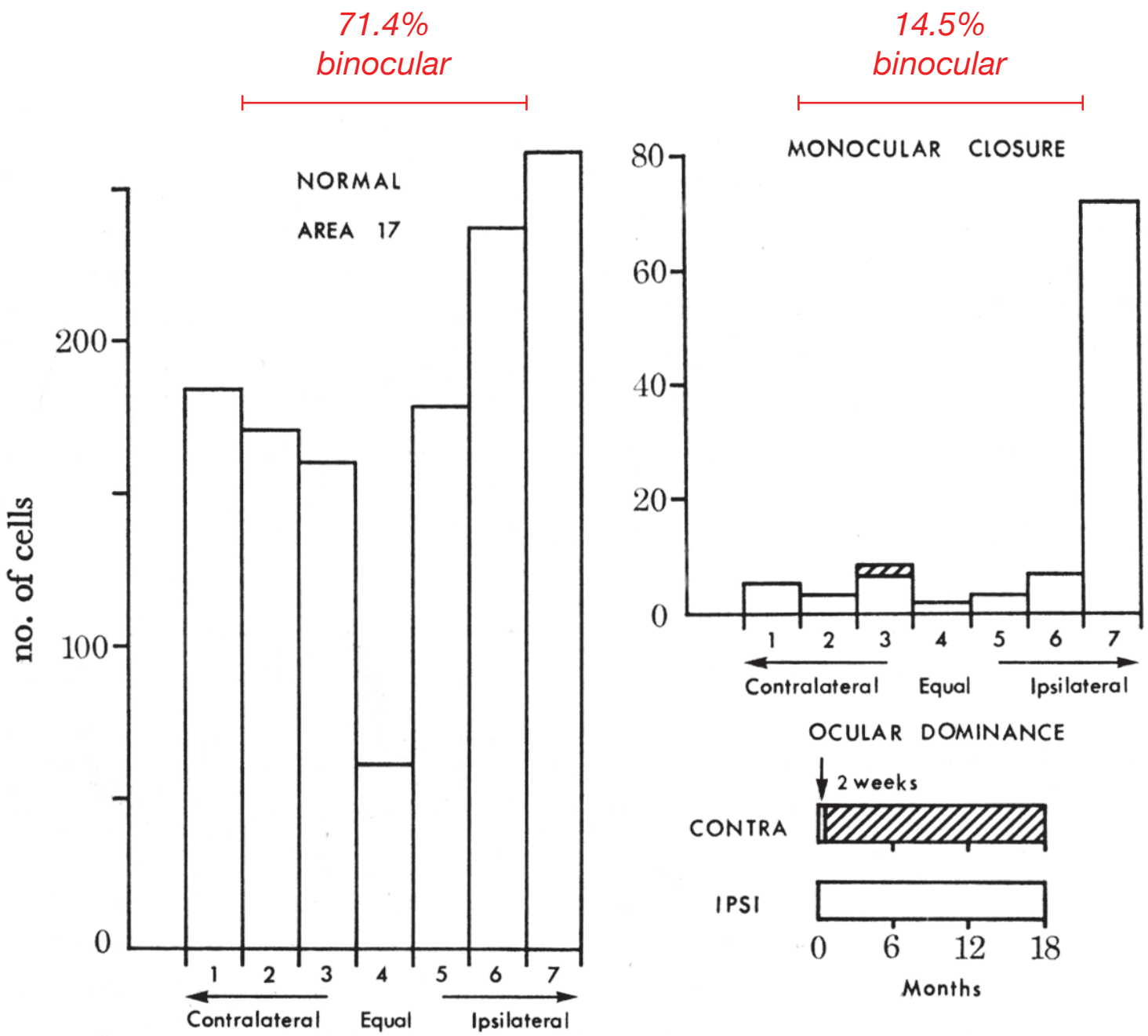

Hubel, Wiesel & LeVay, 1977

Monocular deprivation – mouse

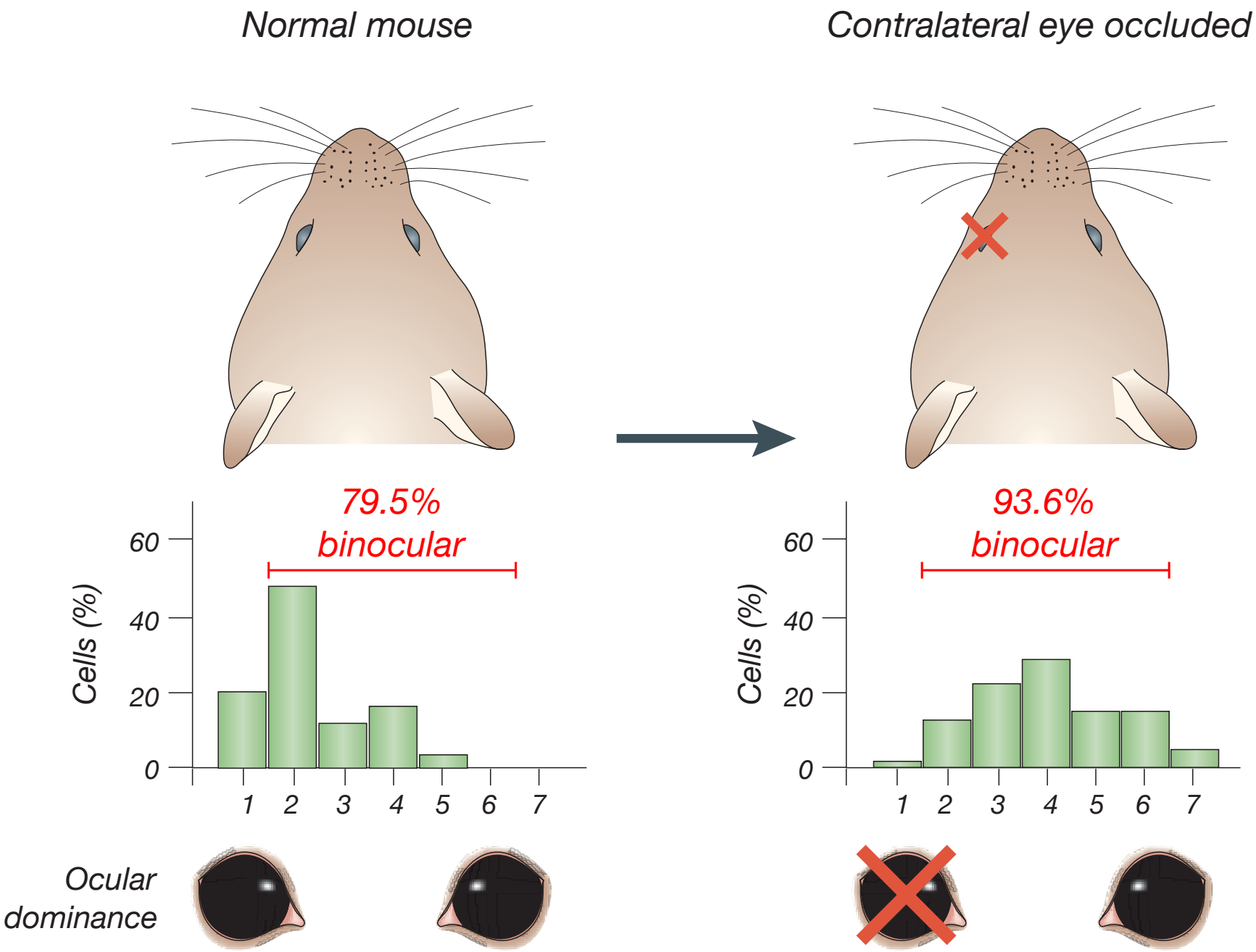

Hensch, 2005

doi:10.1038/nature12153

Rats maintain an overhead binocular field at the expense of constant fusion

Damian J. Wallace[1]*, David S. Greenberg[1]*, Juergen Sawinski[1]*, Stefanie Rulla[1], Giuseppe Notaro[1,2] & Jason N. D. Kerr[1,2]

Fusing left and right eye images into a single view is dependent on precise ocular alignment, which relies on coordinated eye movements. During movements of the head this alignment is maintained by numerous reflexes. Although rodents share with other mammals the key components of eye movement control, the coordination of eye movements in freely moving rodents is unknown. Here we show that movements of the two eyes in freely moving rats differ fundamentally from the precisely controlled eye movements used by other mammals to maintain continuous binocular fusion. The observed eye movements serve to keep the visual fields of the two eyes continuously overlapping above the animal during free movement, but not continuously aligned. Overhead visual stimuli presented to rats freely exploring an open arena evoke an immediate shelter-seeking behaviour, but are ineffective when presented beside the arena. We suggest that continuously overlapping visual fields overhead would be of evolutionary benefit for predator detection by minimizing blind spots.

Wallace et al, 2013

Binocular eye movements

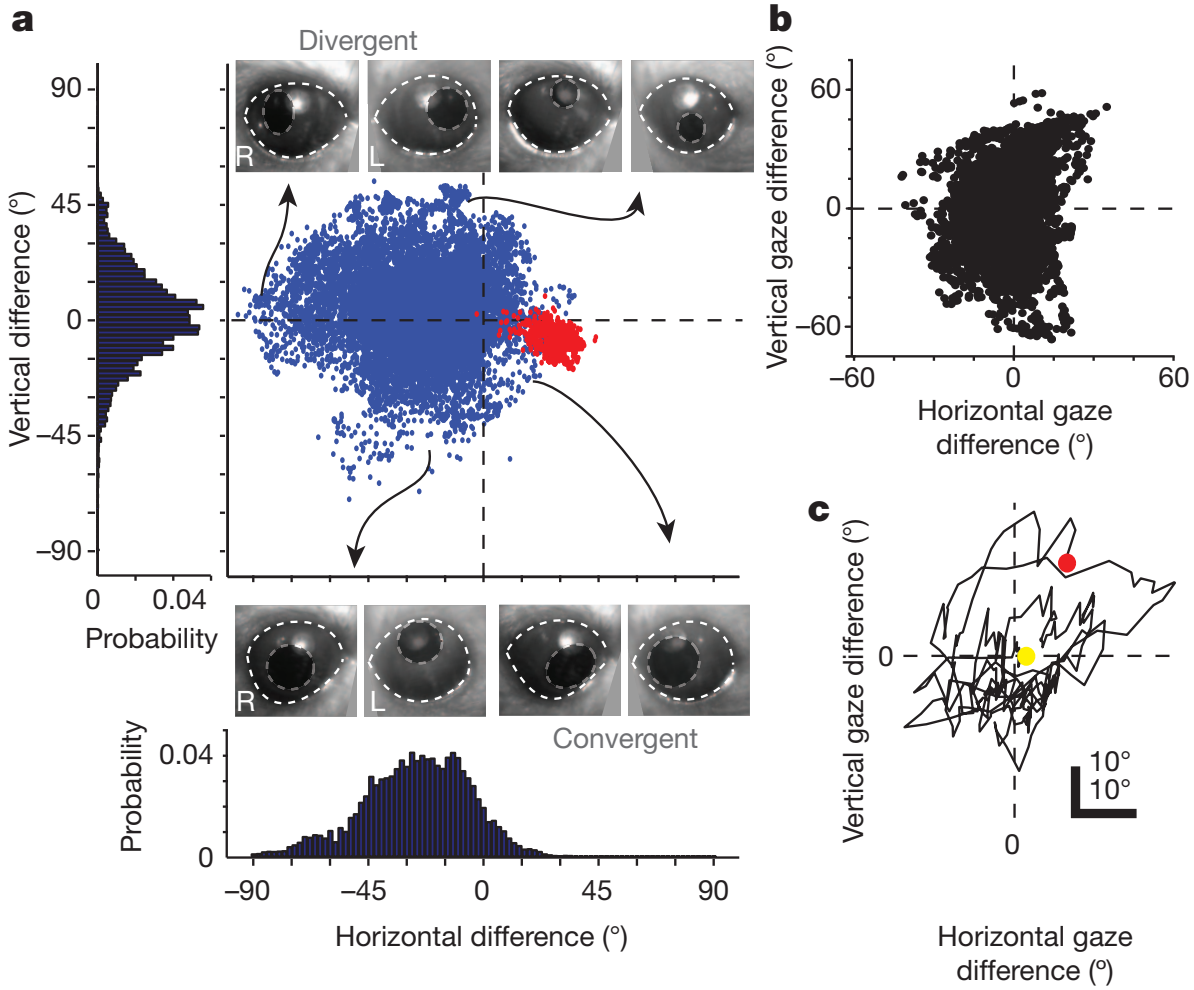

Figure 3 | Asymmetrical eye movements in freely moving rats.
a, Distributions of the difference between left and right eye positions for a freely moving (blue) and head-restrained (red) rat. Each point represents the right eye position minus the left eye position for a single frame. Histograms are shown for *x* and *y* axes. Example image pairs (inset) from positions in the distribution (arrows). Conventions for eye images as in Fig. 1a. **b**, Scatter plot of the difference in left and right eye gaze vectors during free movement. **c**, Plot of the difference in left and right eye gaze vectors during free movement for a single continuous 1.7 s data segment including a gap cross.

Wallace et al, 2013

Binocular eye movements

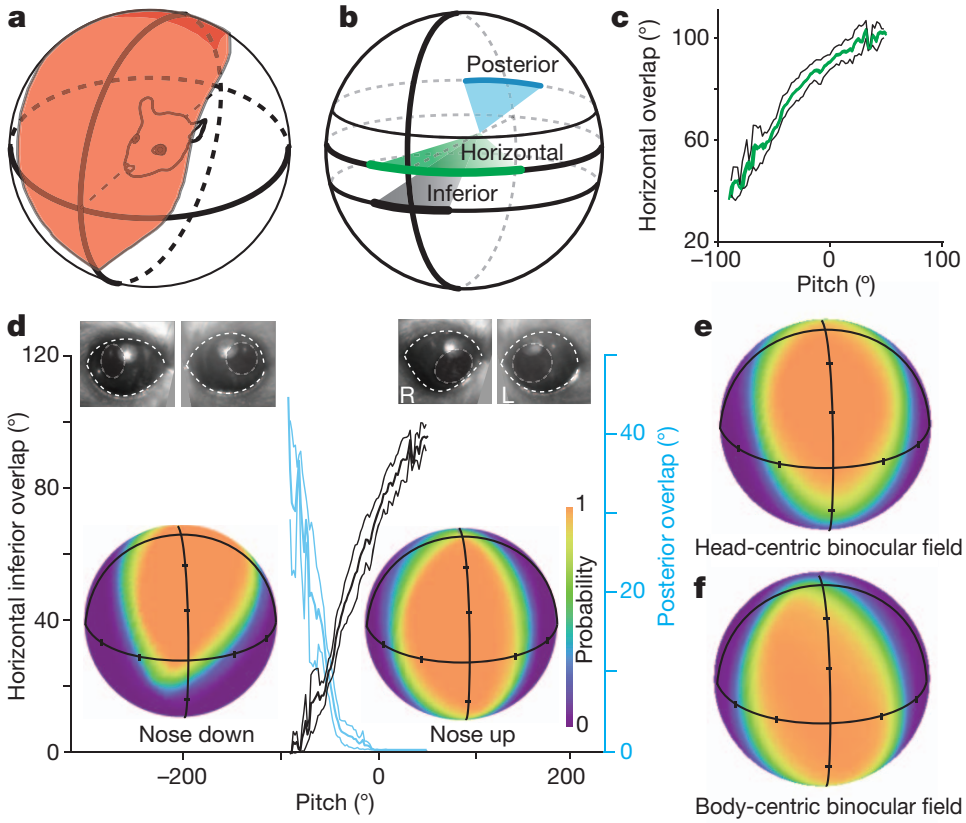

Figure 5 | Overhead binocular overlap. **a**, Schematic outlining binocular overlap (red, modified from ref. 1). **b**, Schematic for data in **c** and **d**. **c**, Average (green) dependence of horizontal overlap on head pitch (s.e.m., thin black lines, $n = 4$ animals). **d**, Dependence of horizontal inferior (black) and posterior (blue) overlap on head pitch (s.e.m., thin black lines, $n = 4$ animals). Head-centric density plots (insets) showing probability of visual field overlap (pseudo-colour) when animal is pitched down (≤10th centile of head pitch angles, insert left) or pitched up (≥90th centile, insert right, 30° ticks on vertical and horizontal axes). Note that average head roll was 18 ± 1° during nose-down pitch. Images (upper insets) show example eye positions for negative and positive head pitch (same as in Fig. 3a). **e**, Head-centric density plot of average overlap of monocular visual fields during free movement for all head positions (conventions as in **d**, $n = 4$ animals). **f**, Body-centric density plot of the overlapping fields that includes head and eye movements (conventions as in **d**, **e**, $n = 4$ animals). See Supplementary Fig. 11 for body-centric definition.

Wallace et al, 2013

Spatial contrast sensitivity of the mouse

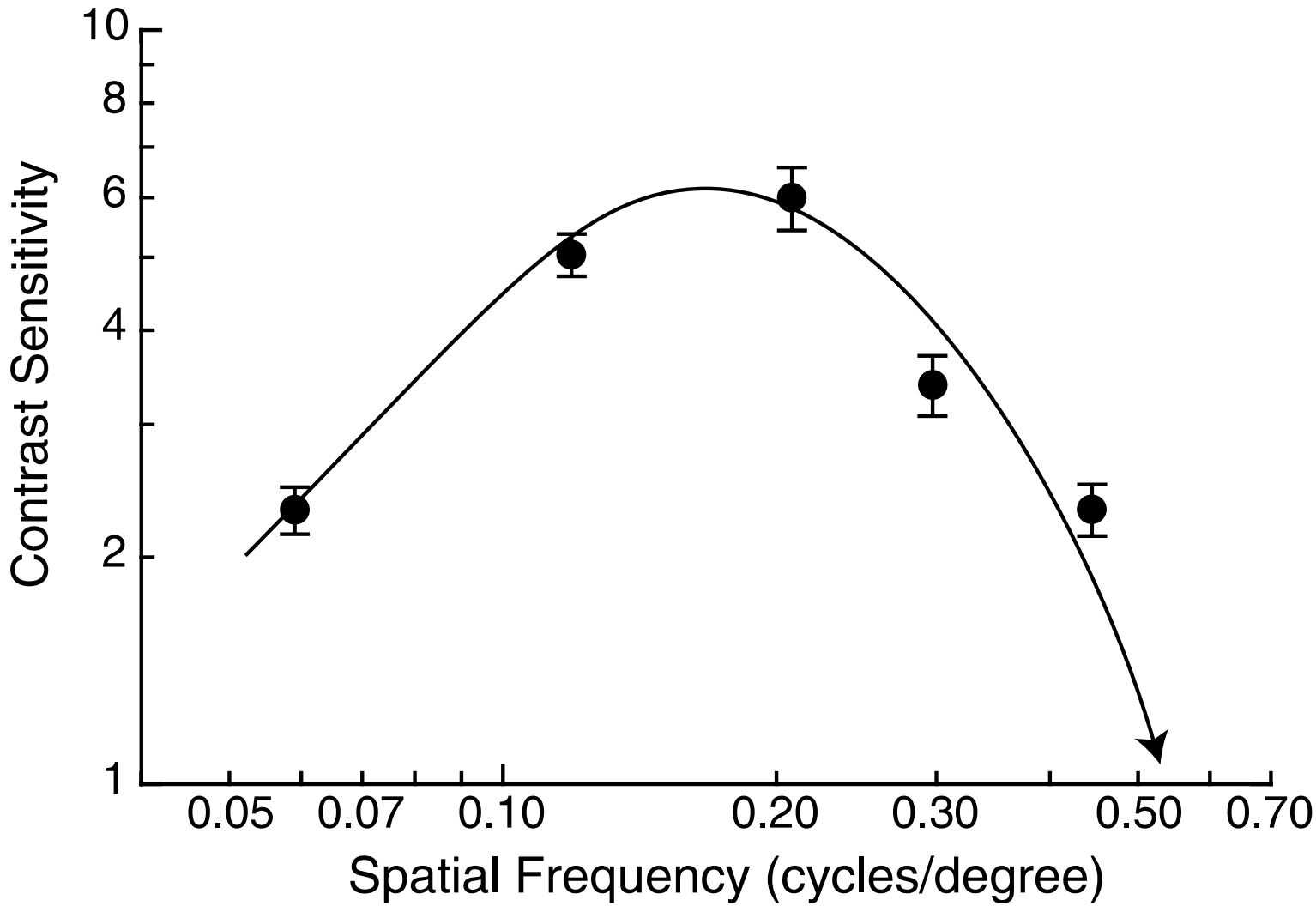

Prusky & Douglas, 2004

Spatial contrast sensitivity of the mouse

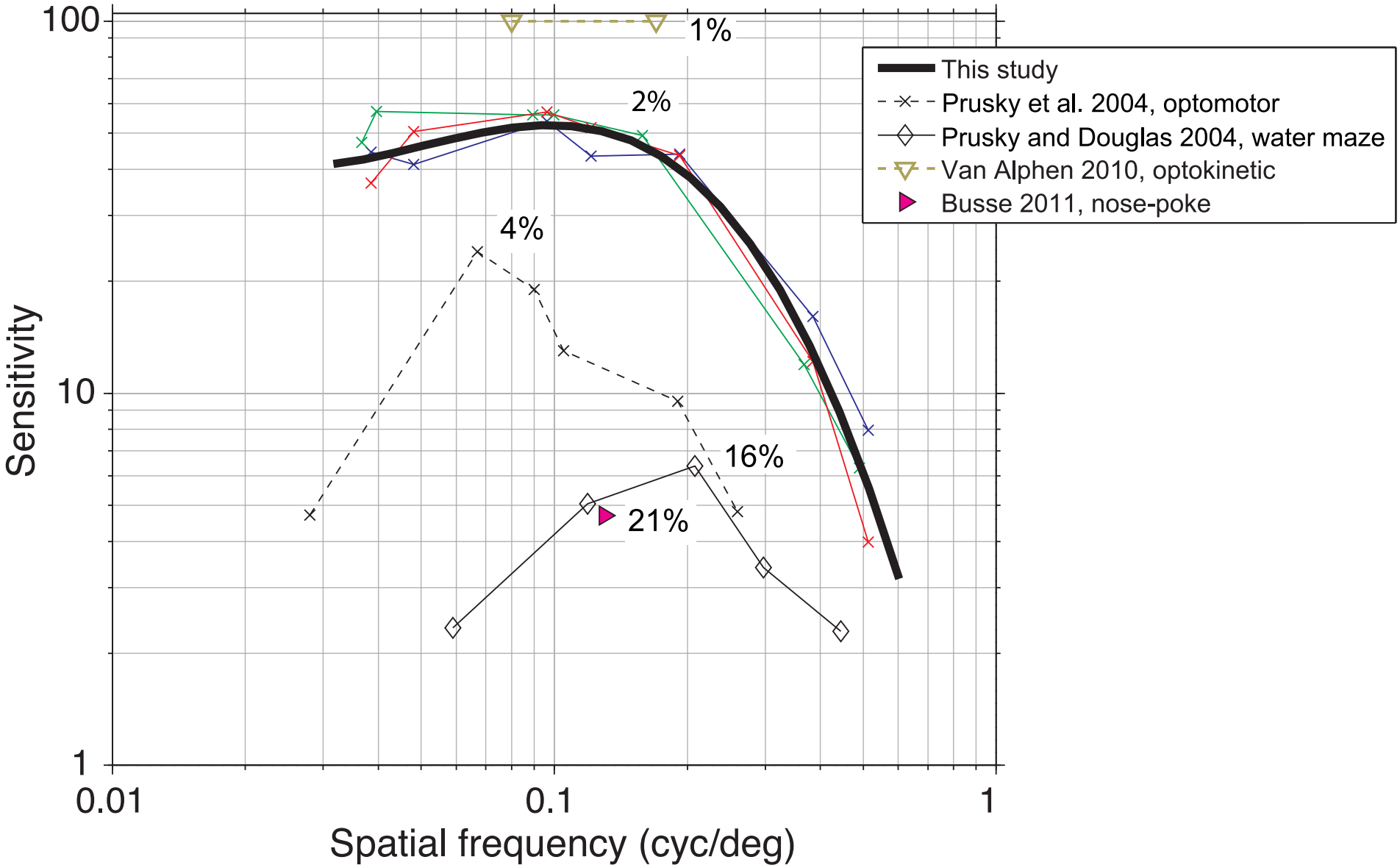

Histed et al., 2012

Spatial contrast sensitivity of the mouse

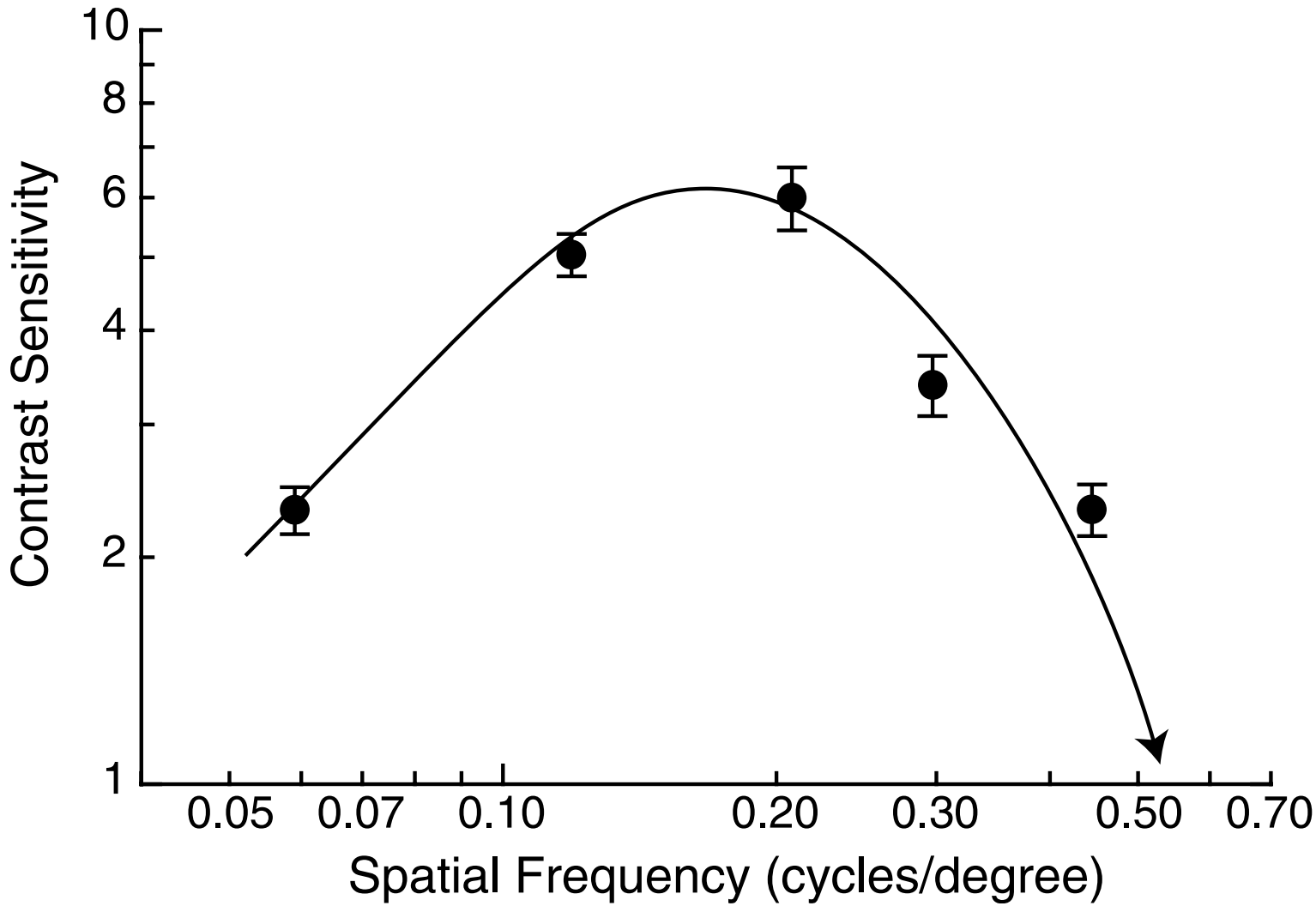

Prusky & Douglas, 2004

Effects of striate cortex removal in mouse

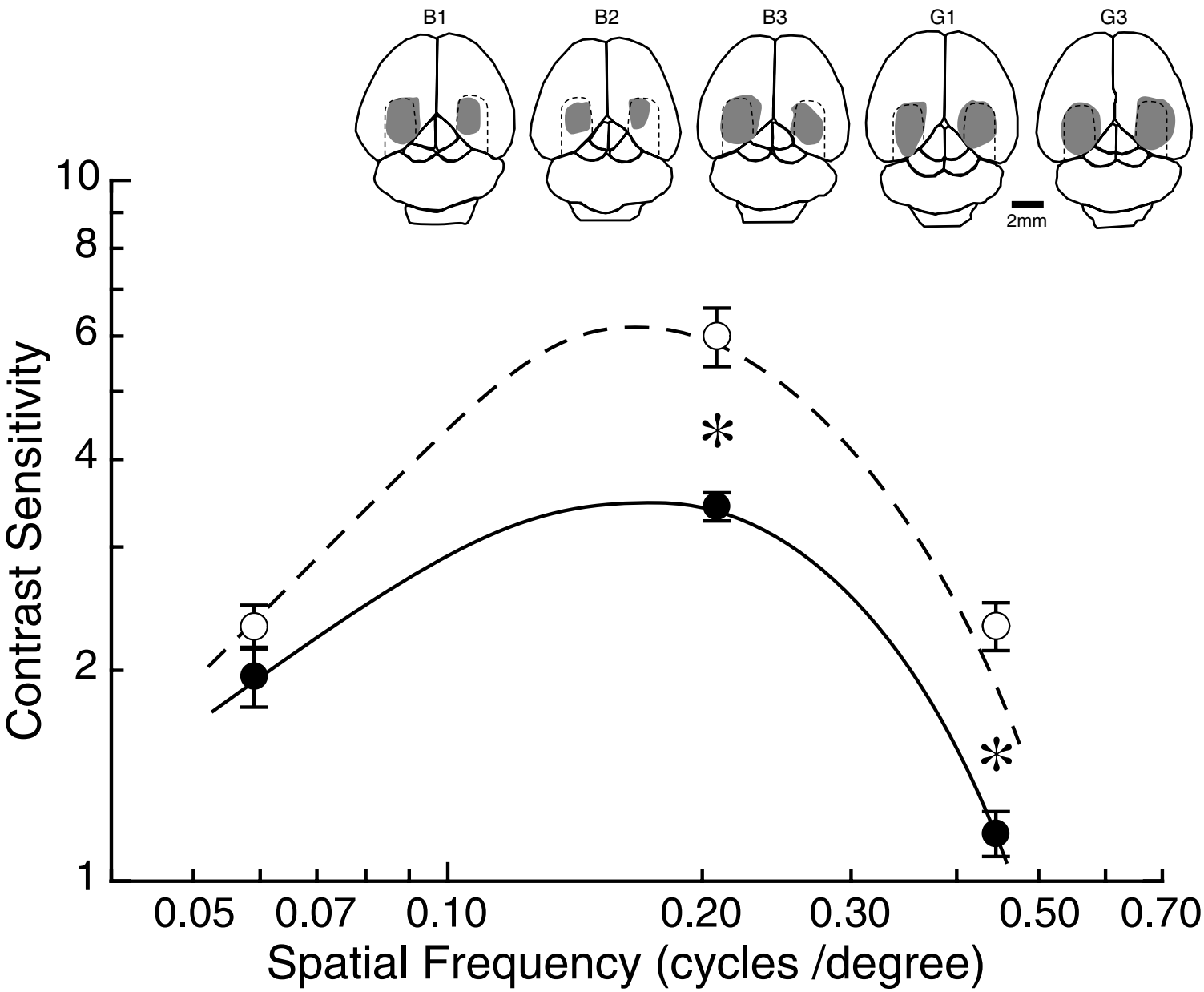

Prusky & Douglas, 2004

Effects of striate cortex removal in monkey

Complete V1 lesion

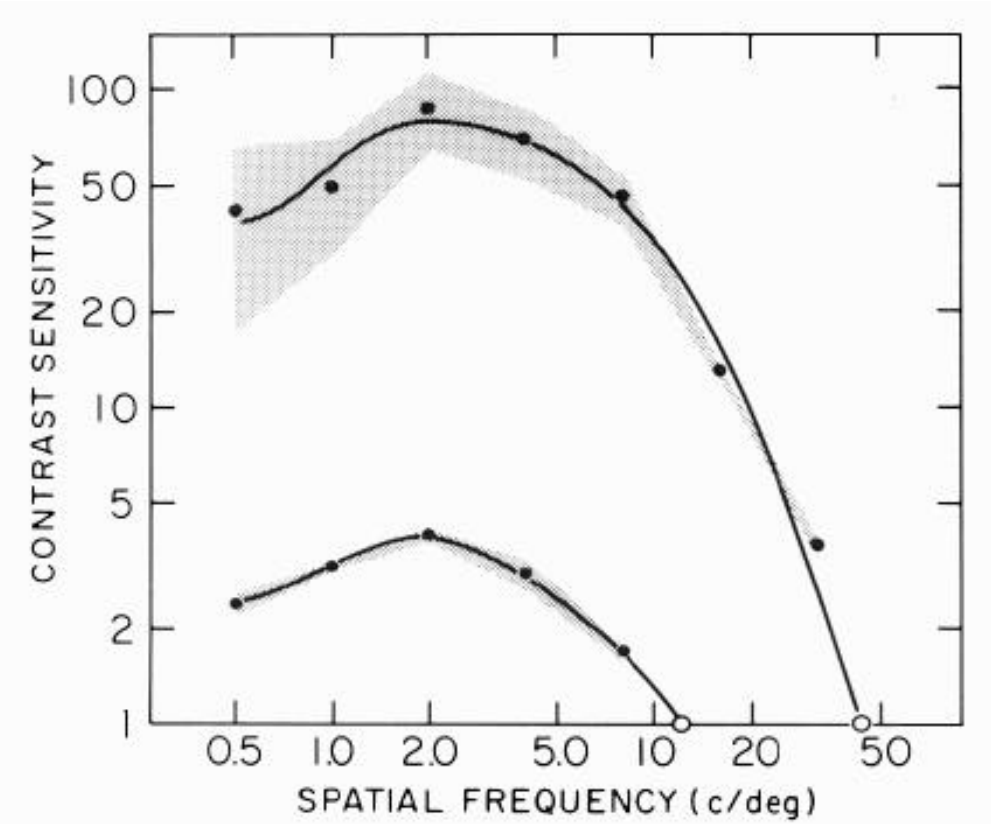

Miller et al., 1980

Focal V1 lesion

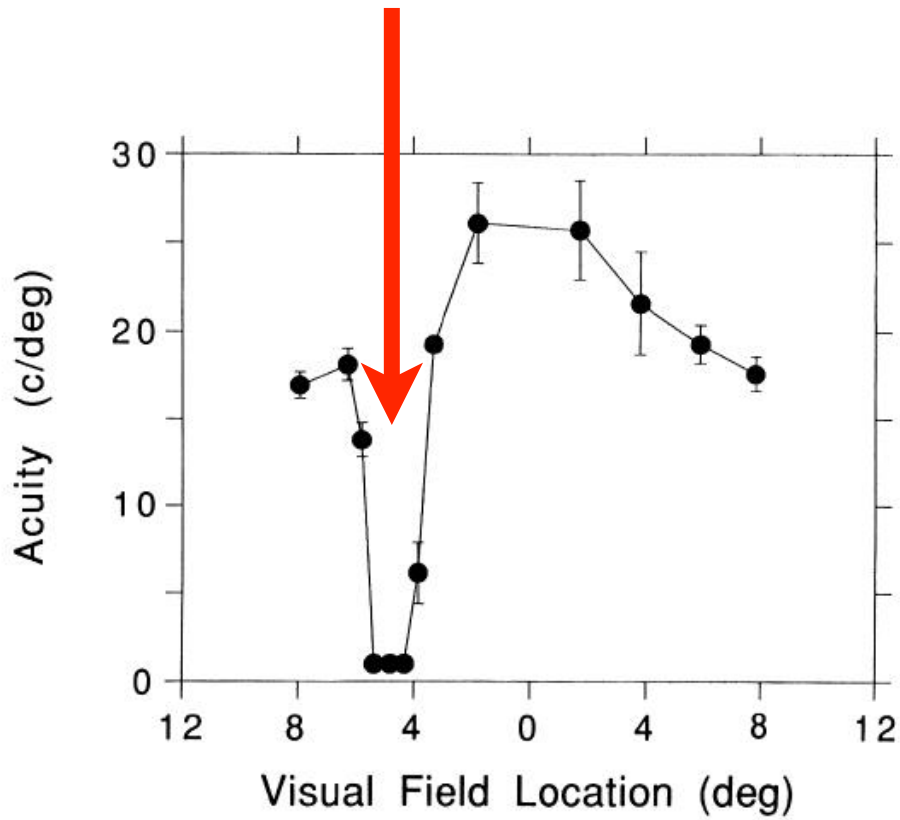

Merigan et al., 1993

Effects of striate cortex removal in monkey and mouse

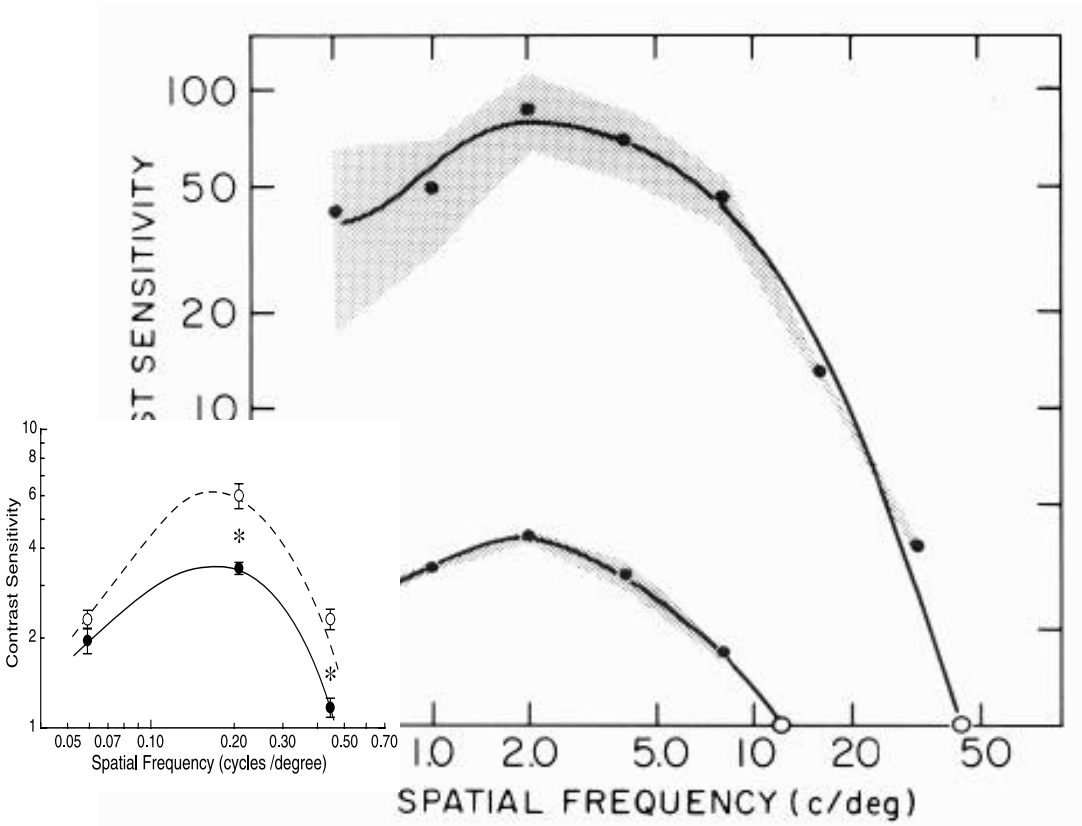

Other rodents may be different
(Lashley, Schneider, ... Reinagel, and many others)

Miller et al., 1980

Effects of striate cortex removal in human

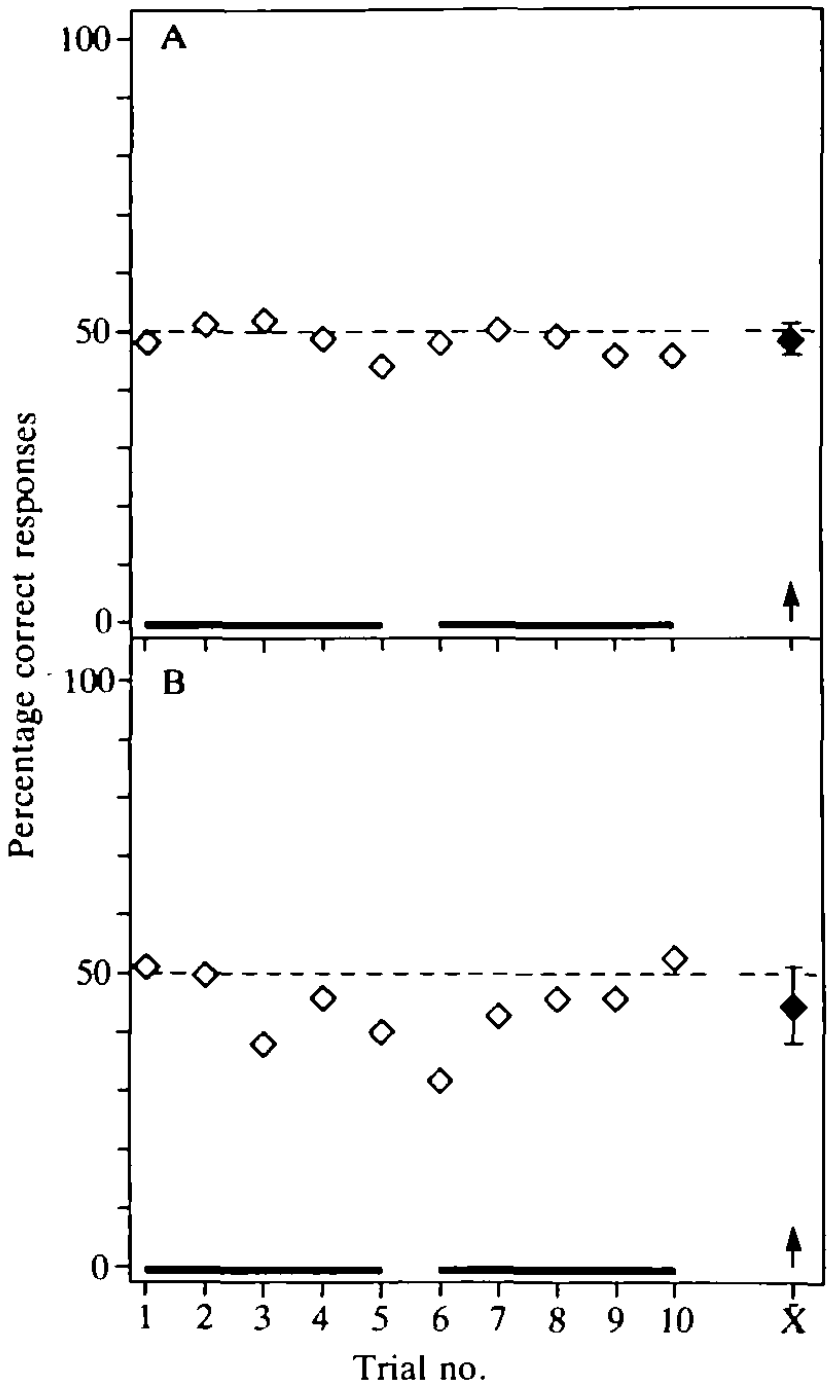

FIG. 20. Result of repeated experimental trials in the perimetrically-blind hemifield of *Case 1*. The data were generated in two series of 5 × 100 frequency of seeing trials at each of two contrast levels. A, results of trials at 90% contrast; B, of trials at 30% contrast. The test location for all trials was 20° eccentric in the perimetrically-blind hemifield. Temporal modulation frequency was 5 Hz, corresponding to this subject's peak modulation response at the same eccentricity in the sighted hemifield (*see* fig. 11A). The isolated datum point indicated by a vertical arrow to the right of the abscissa in both A and B is the mean (± 1 SD) of the total of 10 × 100 trials.

Hess & Pointer, 1989

Intrinsic cortical connections in macaque

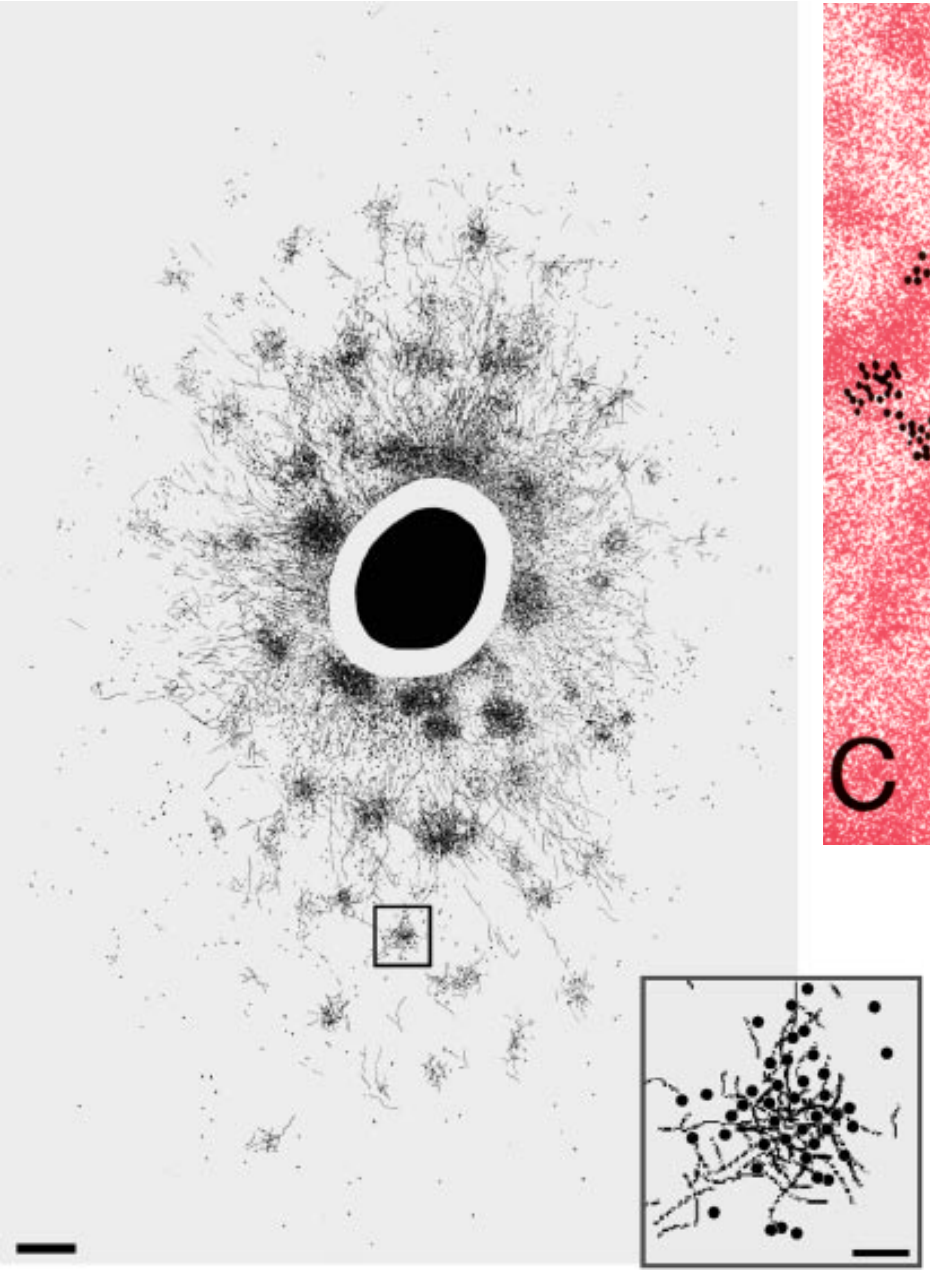

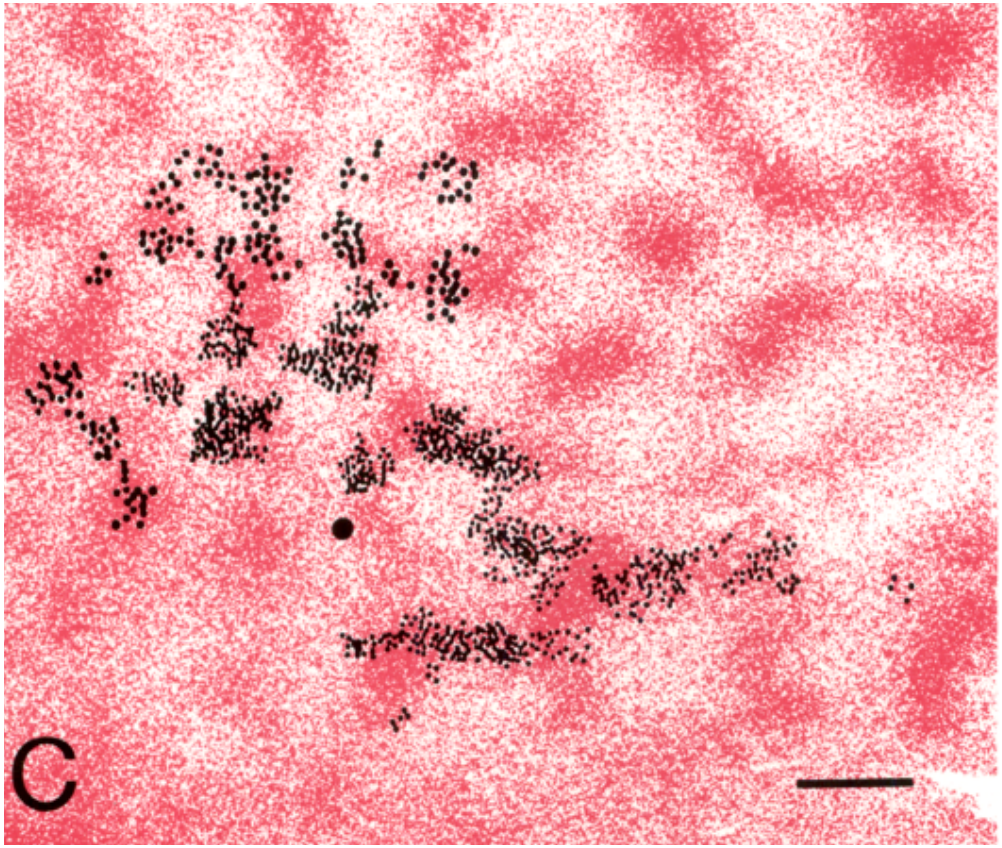

Angelucci et al., 2002; Gilbert & Wiesel, 1989

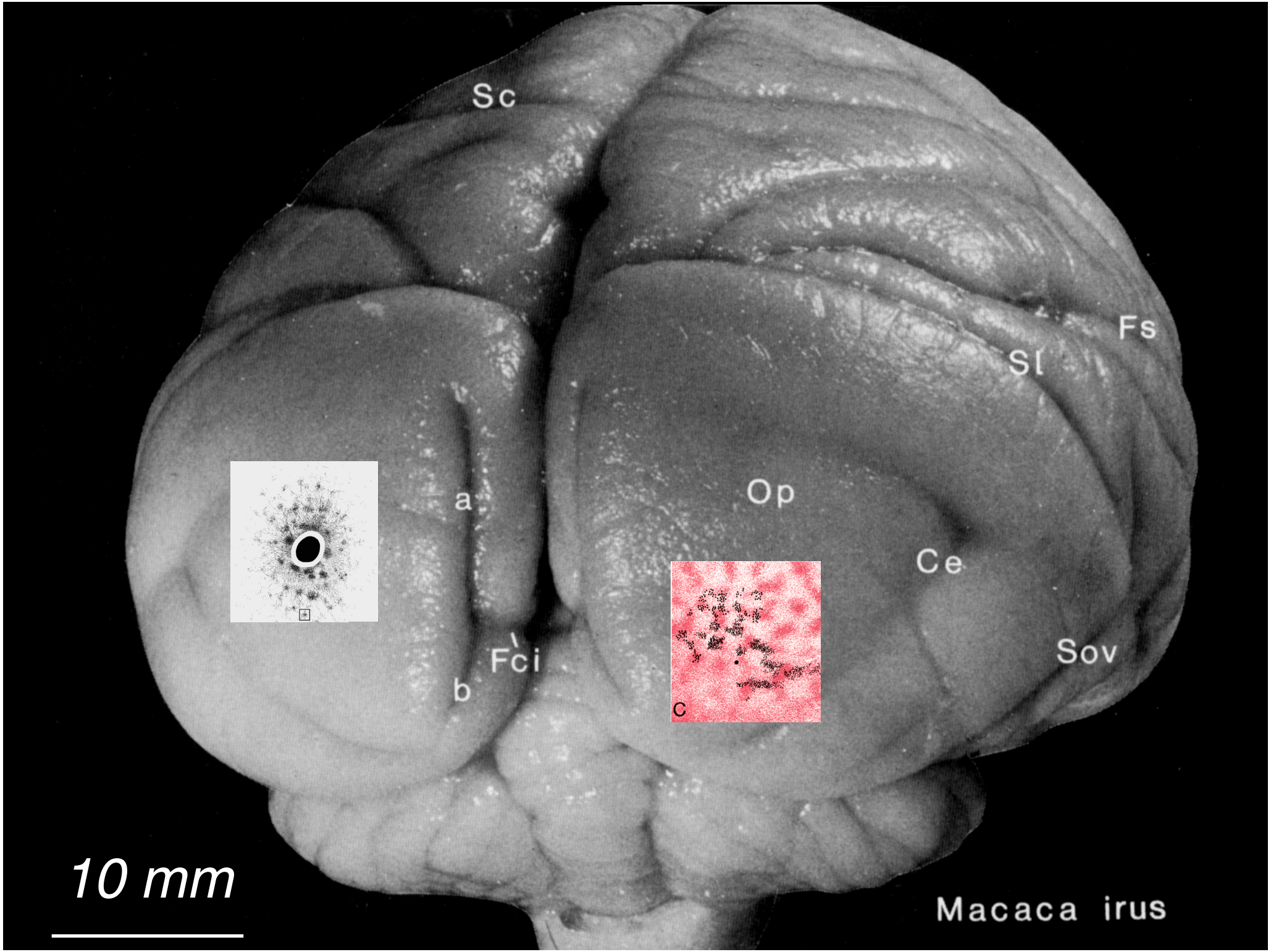
Sc
Fs
Sl
Op
Ce
Sov
a
b
Fci
c
10 mm
Macaca irus

Local connectivity of macaque V1

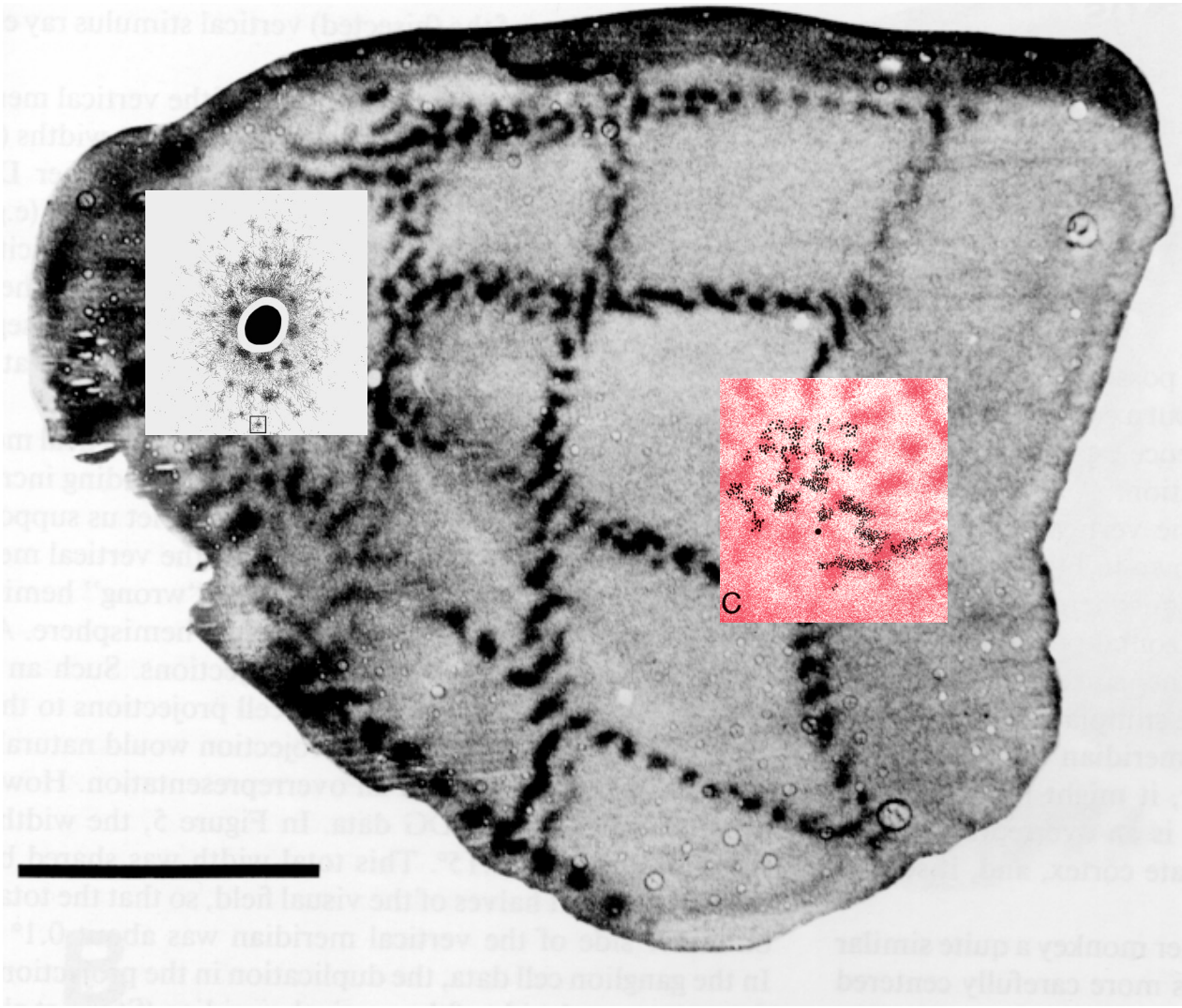

Tootell, Silverman, Switkes and DeValois, 1982

Cortical connections in mouse

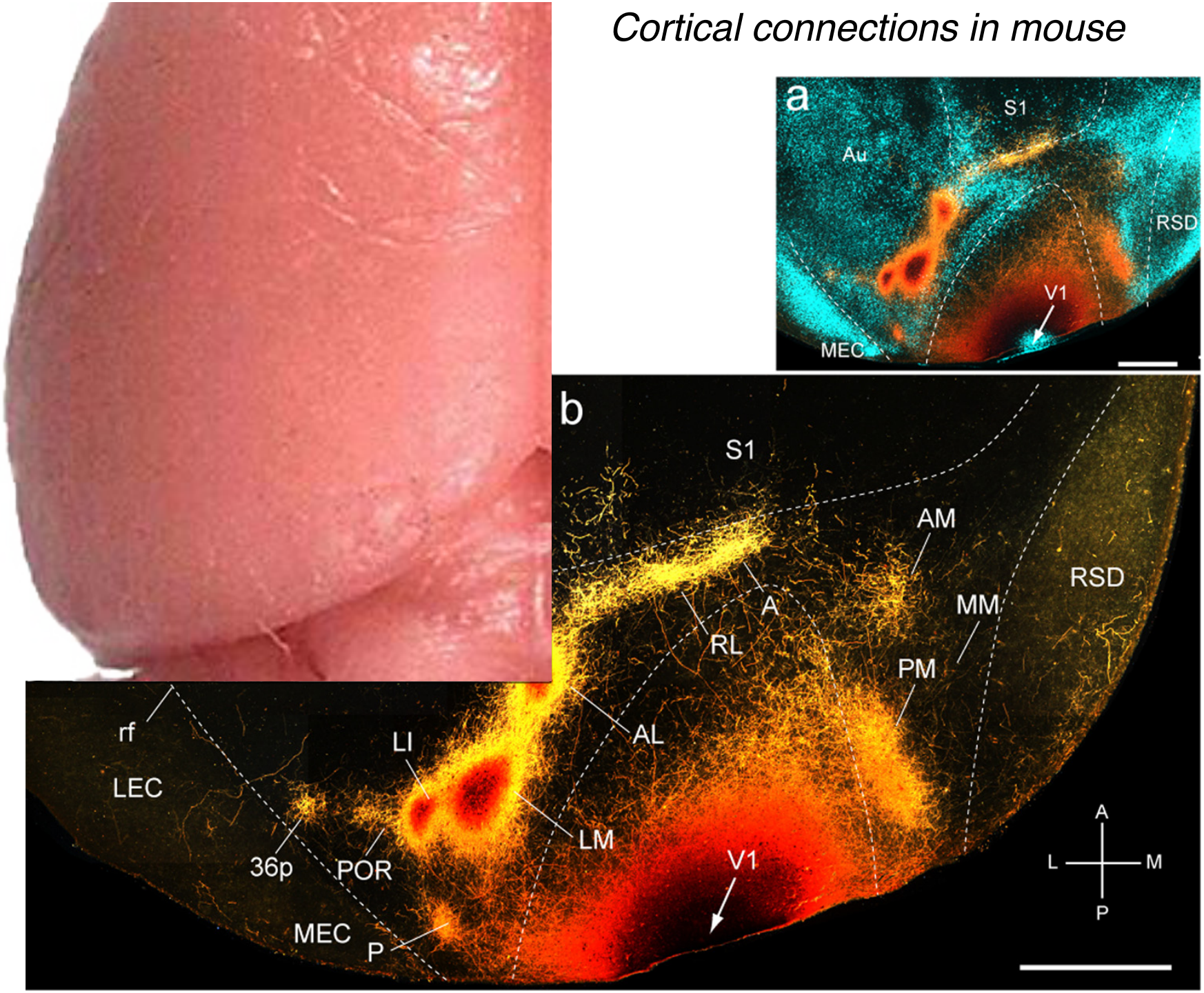

Wang, Sporns & Burkhalter, 2012

Response properties in mouse cortex

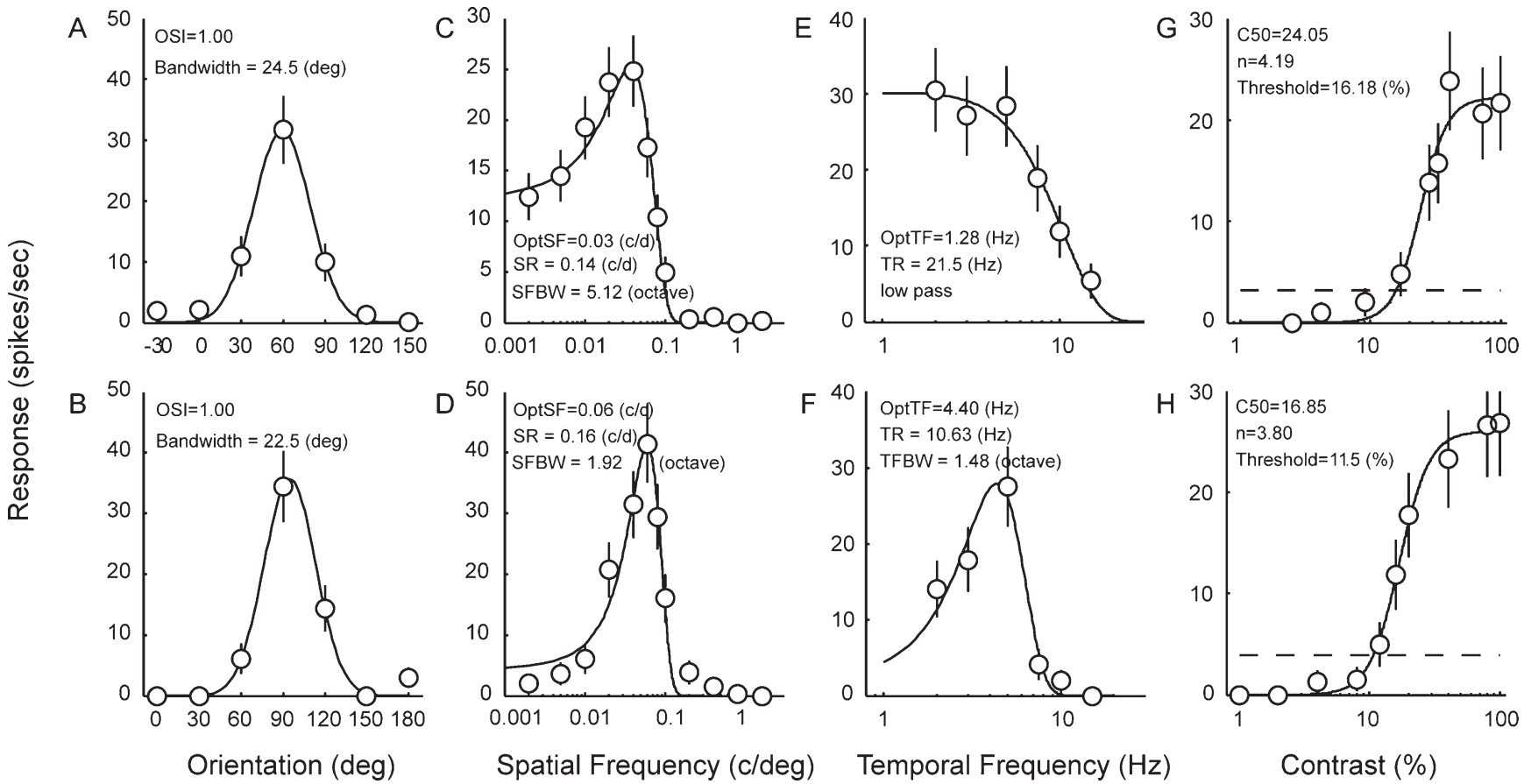

Figure 3. Representative tuning curves for stimulus orientation (**A,B**), spatial frequency (**C,D**), temporal frequency (**E,F**), and contrast (**G,H**) in mice.

Van den Bergh et al, 2010

Response properties in mouse cortex

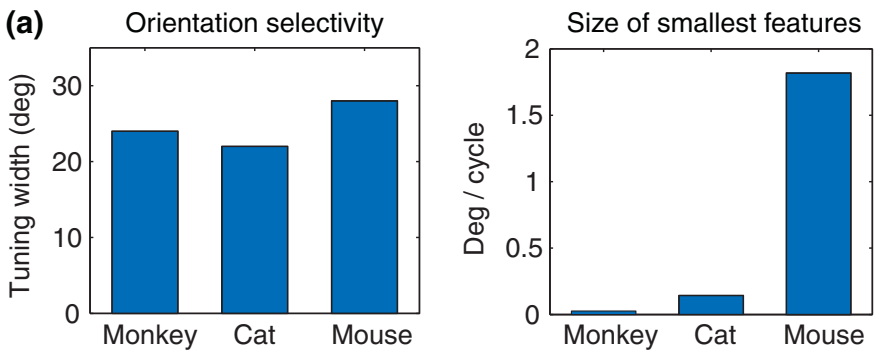

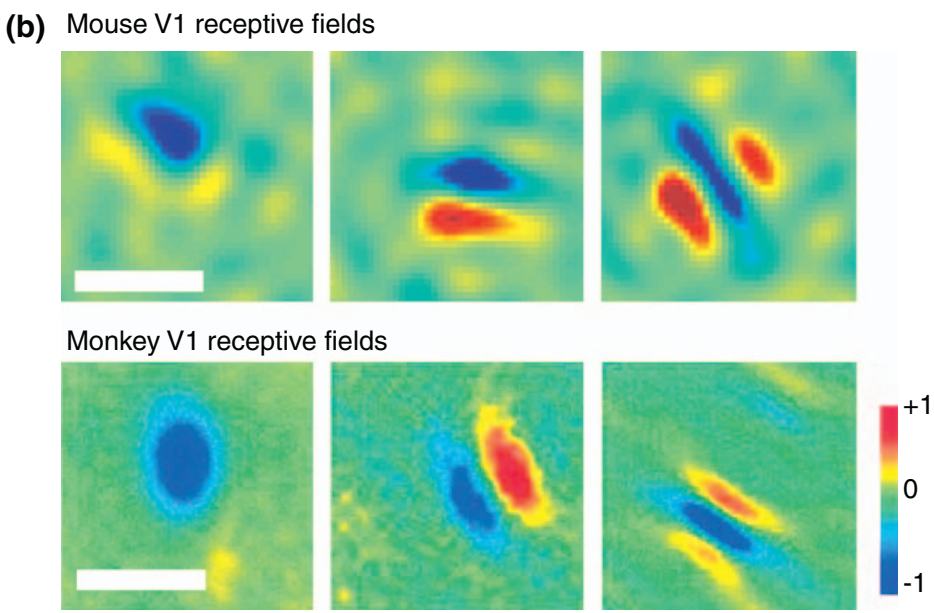

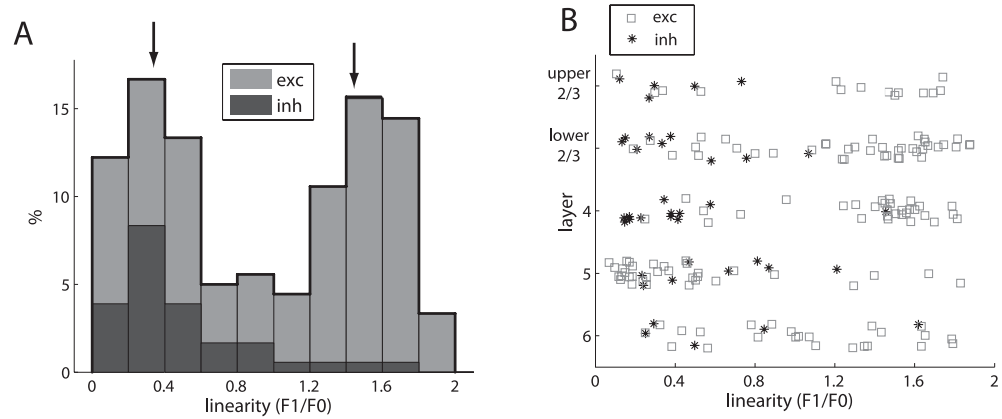

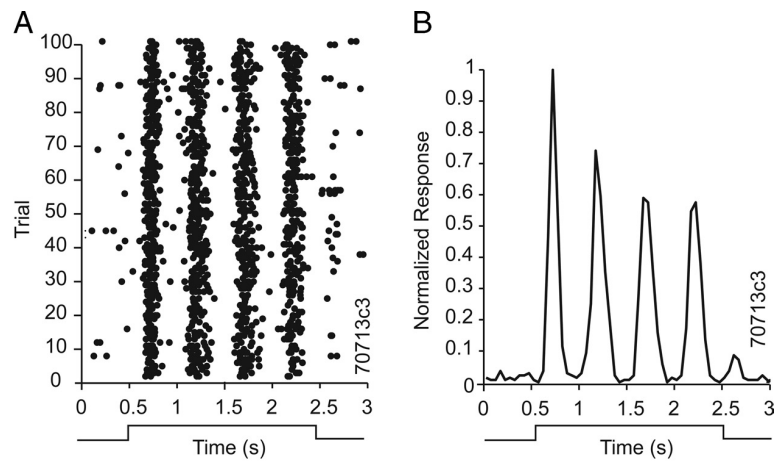

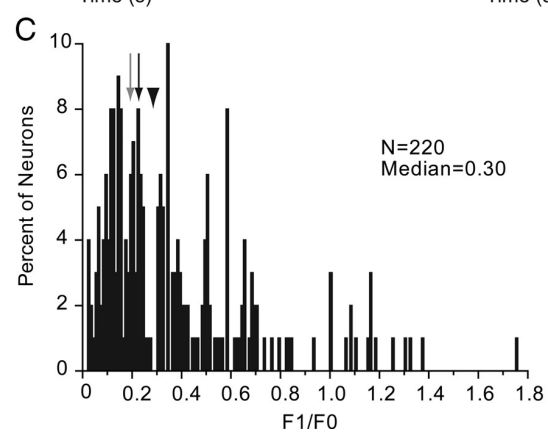

Huberman & Niell, 2011; Niell & Stryker, 2008; Gao et al, 2010

Response properties in mouse cortex

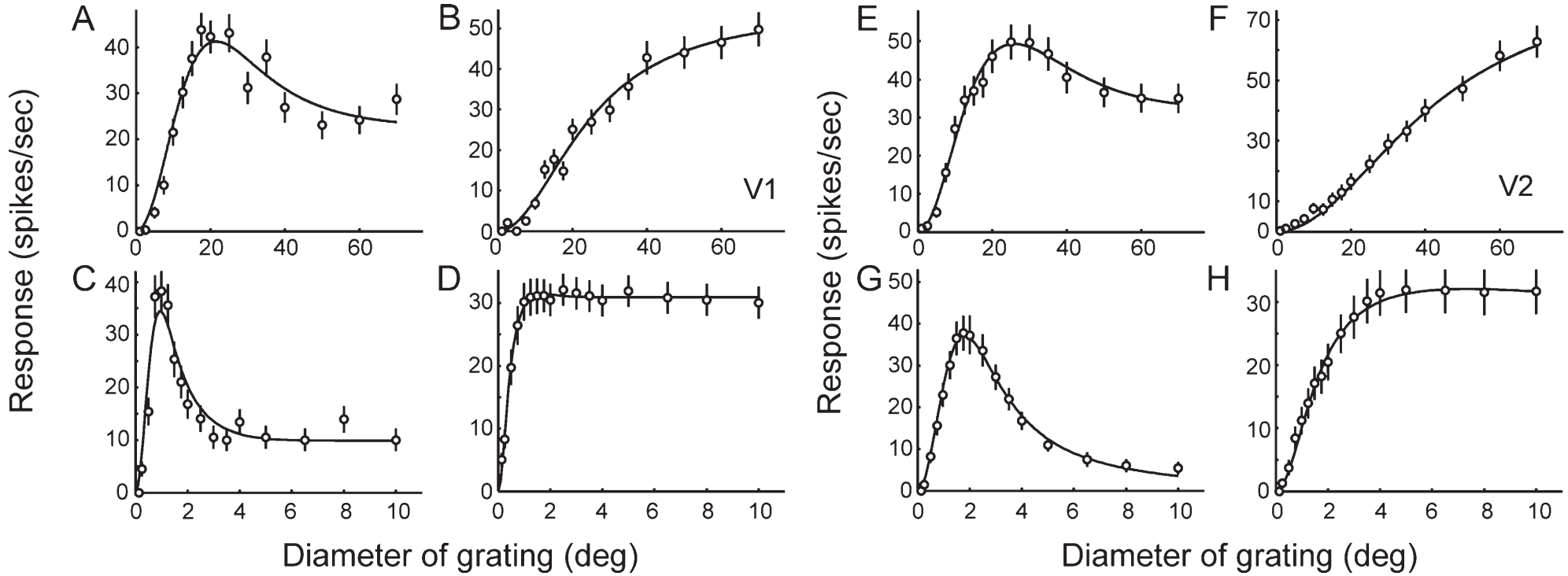

Figure 9. Representative size tuning functions of V1 (**A–D**) and V2 neurons (**E–H**) in mice (top: A,B,E,F) and macaque monkeys (bottom: C,D,G,H). Data points were fitted with the ratios of Gaussians (Cavanaugh et al., 2002). For each species, units with and without surround suppression are illustrated.

Van den Bergh et al, 2010


Understanding of the functional organization of visual cortex started when people recognized that neurons in inferotemporal cortex were doing things that neurons in V1 weren't doing. That observation fell into place largely because V1 and IT are very far apart on many dimensions. Looking for understanding of functional organization in a brain the size of a mouse's, which has to cram all of it limited capacities into a tiny volume, is like working with one hand tied behind our backs.
John Maunsell

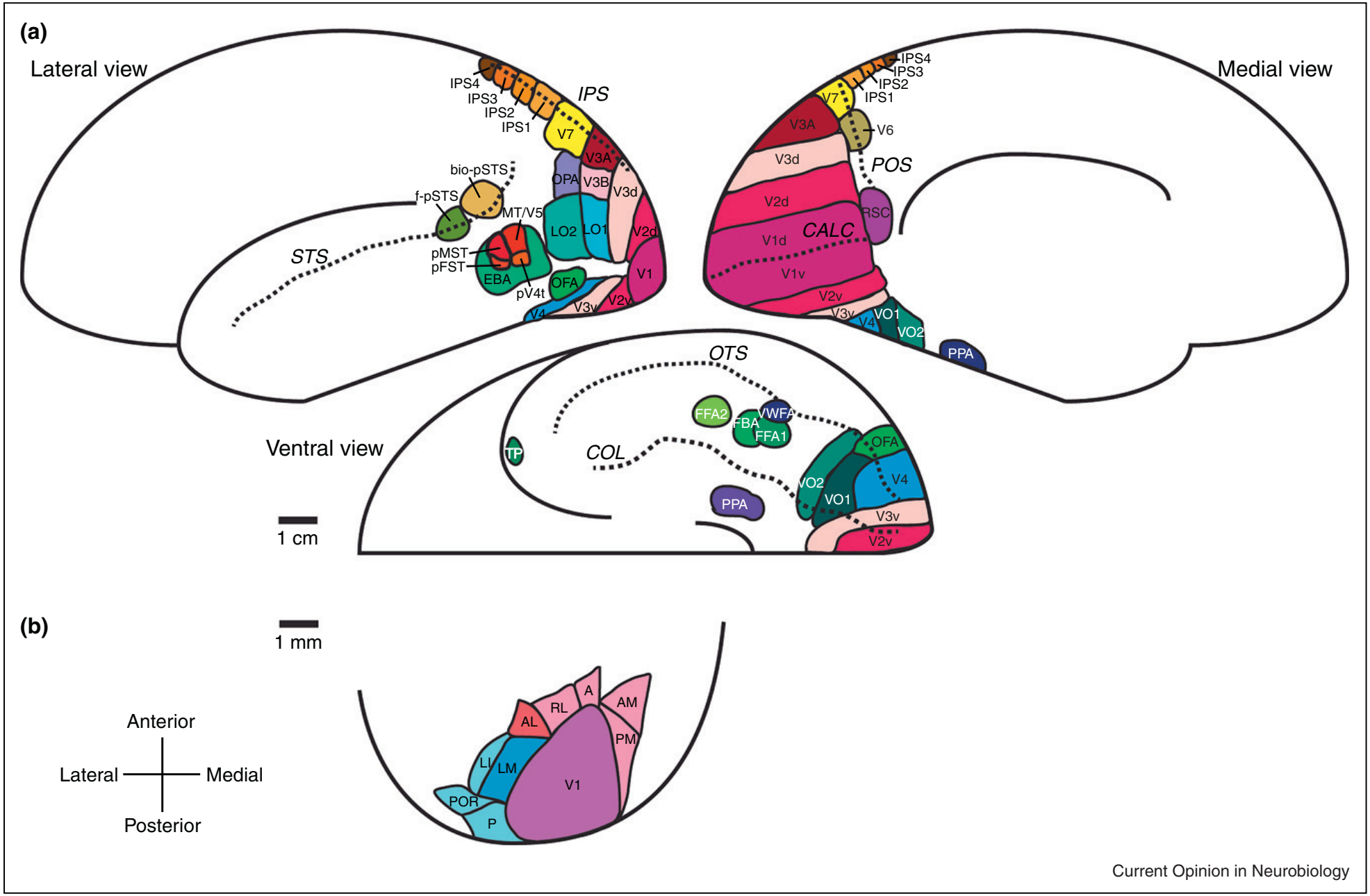

Current Opinion in Neurobiology

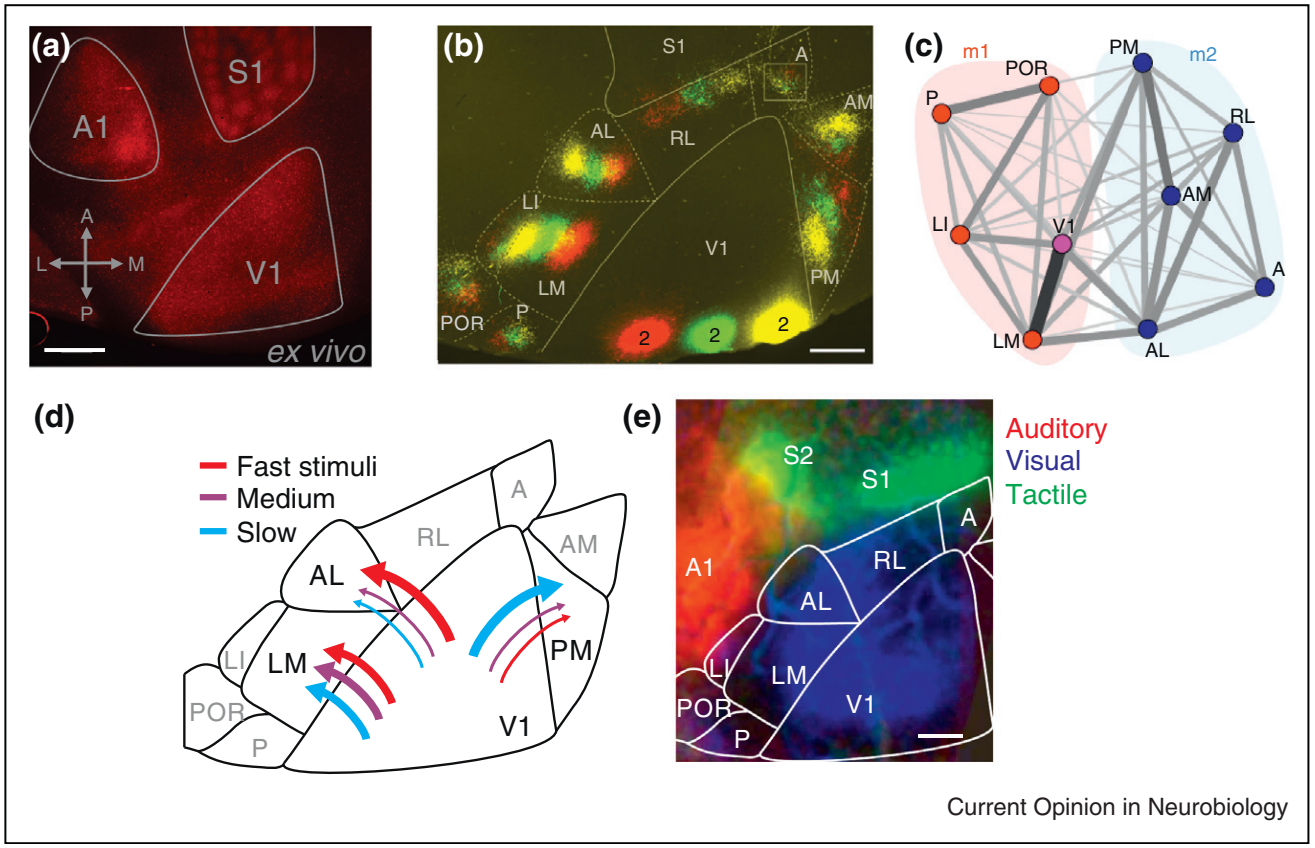

Anatomical and functional organization of mouse visual cortex. **(a)** Fluorescent images from a mouse expressing td-Tomato in parvalbumin positive interneurons (*PV-cre*:Ai9 mice) from a flatmount *ex vivo* section. Td-Tomato expression highlights primary sensory areas (V1 — primary visual cortex; S1 — primary somatosensory cortex; A1 — primary auditory cortex). Data courtesy of D. Roumis. **(b)** Anterograde labeling of V1 projection neurons via fluorescently conjugated dextran injections reveal retinotopically organized arborizations within the higher visual areas. Adapted with permission from Wang and Burkhalter, 2007. **(c)** Connectivity matrix between V1 and nine higher visual areas. Thickness of lines represents the average reciprocal connectivity between areas as measured by the density of axonal projections. Areas are divided into two functional modules: ventral (m1, red) and dorsal (m2, blue). Adapted with permission from Wang, Sporns and Burkhalter, 2012. **(d)** Projections from the same region within V1 to the higher visual areas carry distinct visual information; namely, projections to AL prefer stimuli moving at fast (red) speeds while those to PM prefer slow (blue) speeds. LM receives comparatively diverse input from V1; this could explain the increased anatomical density of this projection. (e) Pseudocolor map of cortical regions sensitive to auditory (red), visual (blue) and tactile (green) stimulation. Note that lateral area LI responds to both visual and auditory stimuli. Area labels were determined by tonotopy, somatotopy and retinotopy. Data courtesy of N. Jikomes. All scales: 500 um.

Extrastriate visual areas in macaque and mouse

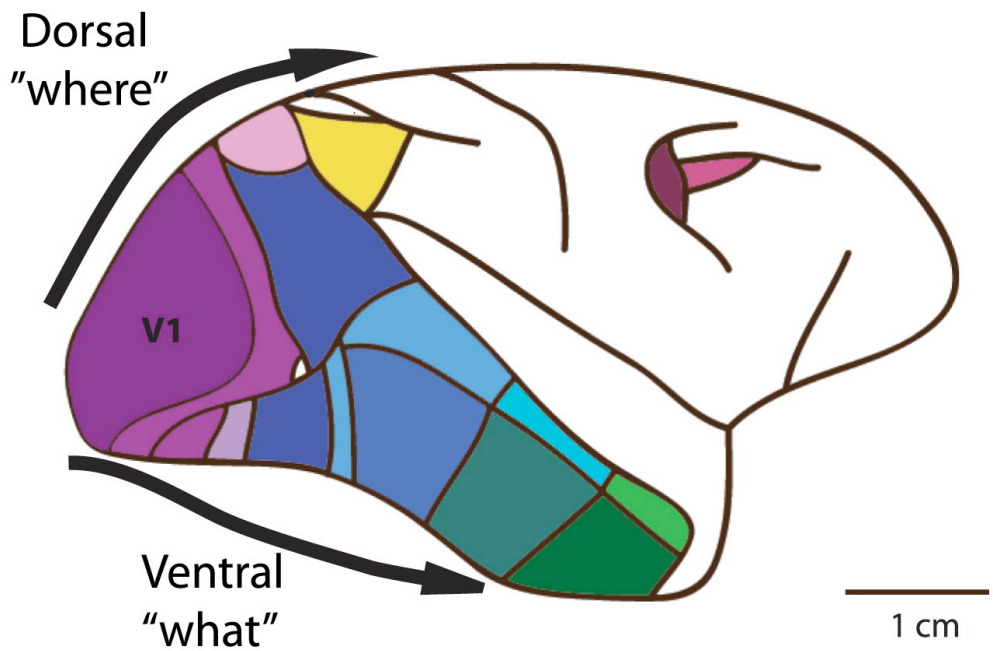

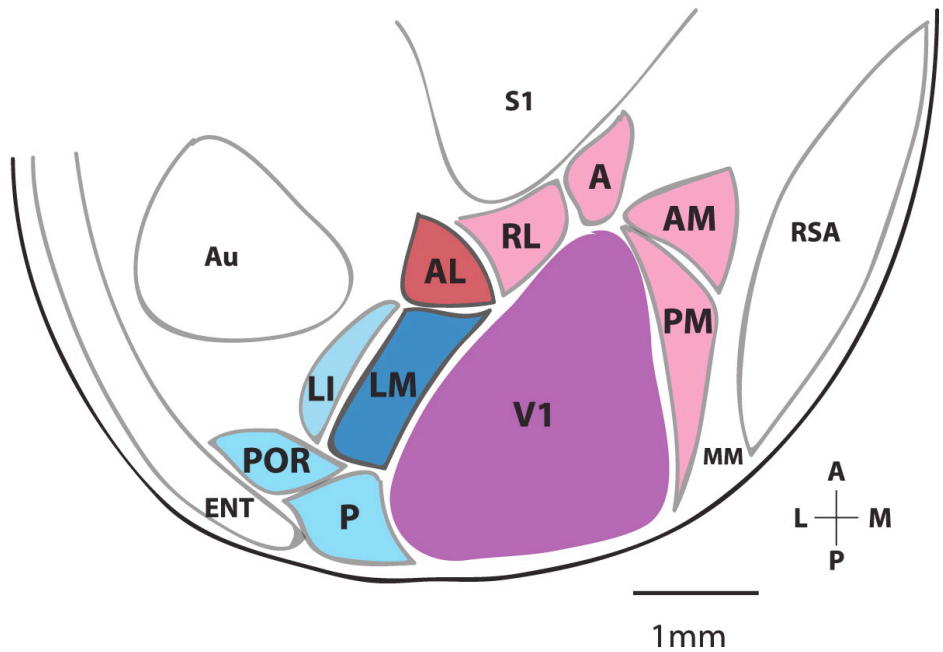

Niell, 2011, after Burkhalter and others

Extrastriate visual areas in mouse

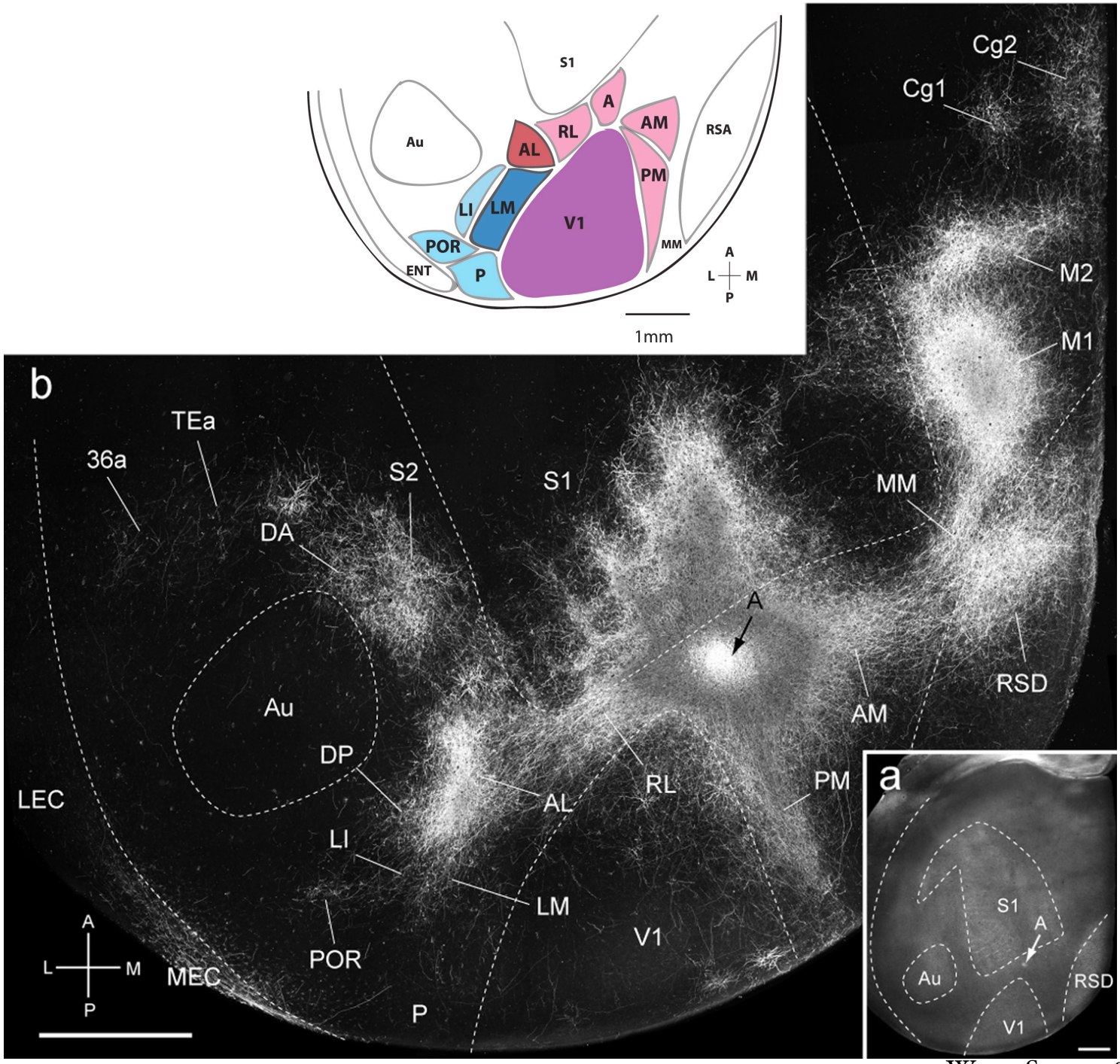

Wang, Sporns & Burkhalter, 2012

Extrastriate visual areas in mouse

	Mean OSI	Mean DSI	Pref. SF (cpd)	Pref. TF (Hz)
V1	0.5	0.26	0.045	0.69
LM	0.55	0.27	0.028	1.8
LI	0.56	0.28	0.04	1.5
AL	0.72	0.35	0.022	1.2
RL	0.69	0.35	0.025	1.3
AM	0.81	0.38	0.033	1.6
PM	0.67	0.29	0.046	0.87

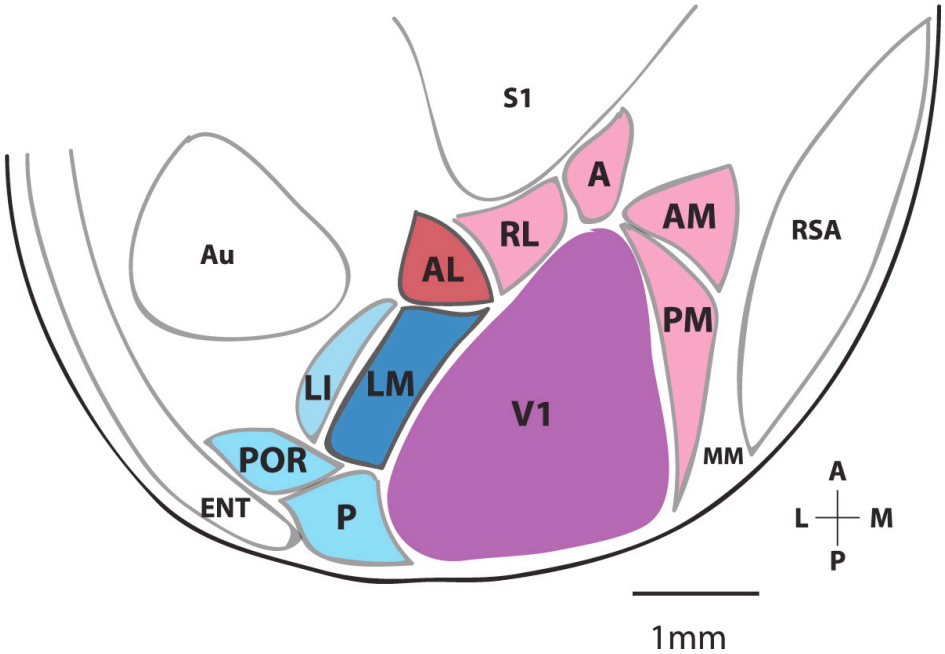

Marshel et al., 2011; Niell, 2011

Mouse cortex is hyperconnected

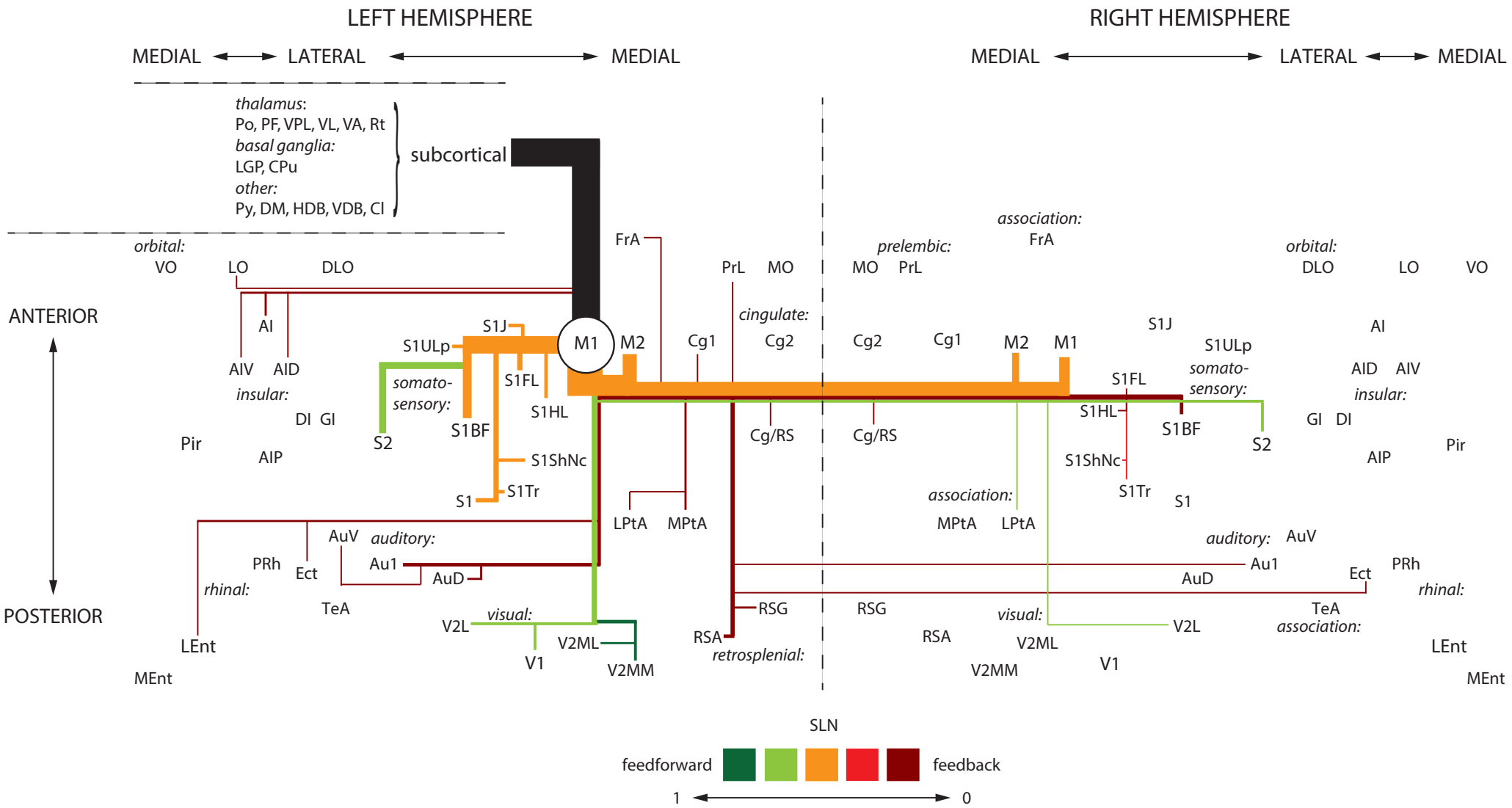

Kevan Martin